

Original Article

Artemisinin derivatives maintain fibroblast normalization by acting on tumor-stroma interactions in oral tongue squamous cell carcinoma

Weixing Zeng^{1,2,3}, Yawen Yang^{1,2,3}, Jia Xiong^{1,5}, Cui Li⁴, Yang He^{1,2,3,6}, Zhihao Liang³, Yongwen He^{1,2,3}

¹Kunming Medical University, Kunming 650106, Yunnan, China; ²Department of Oral and Maxillofacial Surgery, Kunming Medical University School and Hospital of Stomatology, Kunming 650106, Yunnan, China; ³Yunnan Key Laboratory of Stomatology, Kunming 650106, Yunnan, China; ⁴Technology Transfer and Achievement Incubation Center, Kunming Medical University, Kunming 650504, Yunnan, China; ⁵School of Public Health, Kunming Medical University, Kunming 650500, Yunnan, China; ⁶Department of Stomatology, Taihe Hospital, Hubei University of Medicine, Shiyan 442000, Hubei, China

Received December 10, 2024; Accepted May 30, 2025; Epub June 15, 2025; Published June 30, 2025

Abstract: Fibroblasts can transform into cancer-associated fibroblasts (CAFs) when continuously stimulated by cancer cells, thereby playing a crucial role in cancer progression. Growing evidence indicates that targeted therapy for CAF can influence tumor progression. Dihydroartemisinin (DHA) and artemether (ARM), semisynthetic derivatives of the natural compound artemisinin, have exhibited anticancer effects in various tumors. In this study, we found that tumor cells secreted platelet-derived growth factor-BB (PDGF-BB), which stimulated fibroblasts to transition into the CAF phenotype (cell phenotype and secretory phenotype). CAFs promote Cal-27 cell proliferation by secreting lactate. We focused on the mechanisms by which DHA and ARM affect the tumor-stroma interactions. These findings demonstrated that DHA and ARM effectively suppressed the secretion of PDGF-BB from Cal-27 cells, maintaining the normal state of hOMF and preventing the proliferative effect on Cal-27 cells. These findings were confirmed in xenograft models. Our study showed that artemisinin derivatives prevent the progression of oral tongue squamous cell carcinoma (OTSCC) by inhibiting the production of PDGF-BB in cancer cells to maintain the normal state of fibroblasts, thus providing a potential avenue for targeted OTSCC treatment.

Keywords: Oral squamous cell carcinoma, artemisinin derivatives, PDGF-BB, cancer-associated fibroblasts, normal state

Introduction

Oral squamous cell carcinoma (OSCC) is a common malignant tumor of the head and neck region, originating from the oral cavity's mucosal lining [1]. The cancer accounts for approximately 170,000 deaths annually worldwide [2]. Despite therapeutic advances, no significant improvement has been observed in long-term patient survival, primarily because the role of the tumor microenvironment in cancer development has been overlooked [3, 4]. The association of the TME with cancer growth implicates non-cancerous stromal components in tumor progress, making them viable targets for innovative cancer therapies. Insight into these interactions offers promising therapeutic avenues for improved patient survival [5].

Cancer-associated fibroblasts (CAFs) are mesenchymal cells that constitute the tumor microenvironment (TME) and contribute to tumor progression in several ways [6-8]. These fibroblasts, primarily derived from host cells, transform irreversibly into CAFs under the persistent influence of cancer cells [9]. Various factors in tumors regulate the conversion of fibroblasts to CAFs, with existing studies showing that cytokines and tumor metabolites can induce fibroblast activation [10, 11]. Cancer cells also secrete numerous factors that facilitate this conversion [12]. Moreover, metabolic changes in fibroblasts, particularly the shift towards aerobic glycolysis, are essential for fibroblasts' phenotypic conversion [13]. Normal fibroblasts adopt a CAF phenotype under the influence of tumor cells and key components of the tumor

microenvironment. CAFs promote tumor progression by secreting pro-oncogenic factors.

Platelet-derived growth factor (PDGF) consists of four polypeptides - A, B, C, and D - that form various dimeric combinations, which activate the PDGF α and PDGF β receptors, thereby initiating receptor tyrosine kinase signaling [14, 15]. This activation process facilitates multiple cellular and biological processes. PDGF-BB is mainly associated with tumor initiation and progression in the PDGF family [16]. PDGF-BB plays various roles in tumors, promoting tumor progression by enhancing tumor cell proliferation, inhibiting apoptosis, and mediating the transformation of endothelial cells into CAFs [17-19]. PDGF-BB induces aerobic glycolysis through the HIF-1 α pathway to promote fibroblast transformation to CAFs [20]. PDGF-BB can promote this process through several mechanisms during the transformation of fibroblasts to cancer-associated fibroblasts (CAFs). Therefore, targeted inhibition of PDGF-BB signaling in fibroblasts may offer a potential therapeutic approach for tumor treatment.

Artemisinin is the first-line treatment for malaria [21]. Recently, a series of derivatives, such as dihydroartemisinin (DHA) and artemether (ARM), have been synthesized by modifying the parent structure of artemisinin. These derivatives exhibit good bioactivity and solubility and have emerged as potential therapeutic agents with broad-spectrum anticancer properties [22]. However, owing to the broad anticancer effects of these compounds, their molecular mechanisms are highly complex, and the mechanisms underlying their ability to inhibit tumor progression and metastasis remain unclear [23]. Research has shown that artemisinin derivatives target cyclin-dependent kinases (CDKs) to inhibit cell proliferation [24]. In addition, artemisinin derivatives can induce apoptosis in cancer cells [25]. Artesunate can reduce the expression of HSP70 and Bcl-2 in breast cancer cells and induce caspase-dependent apoptosis [26]. DHA induces apoptosis in melanoma cells through the NOXA-dependent pathway [27]. Artemisinin derivatives can also induce ferroptosis, selectively eliminating cancer cells while protecting normal cells [28, 29]. Interestingly, the tumor microenvironment (TME) is an essential target for cancer treatment, and artemisinin and its derivatives also

play a significant role in regulating TME. It has been shown that DHA can induce the polarization of tumor-associated macrophages (TAMs) towards the M1 phenotype in a dose-dependent manner [30]. DHA can also inhibit the polarization and infiltration of regulatory T cells (Tregs) in the tumor microenvironment by reducing IL-10 and IL-6 levels in melanoma [31]. Additionally, DHA promotes anti-tumor immunity by decreasing Tregs and increasing cytotoxic T cells' infiltration (CD8+) [32]. Artemisinin derivatives also induce leukemia cell apoptosis by inhibiting the JAK2/STAT3 signaling pathway, thereby reducing the number of M2-type macrophages [33]. These compounds interfere with cancer cell growth by targeting specific proteins and cells.

Artemisinin derivatives inhibit tumor growth through various mechanisms, and numerous studies have shown that these derivatives can regulate the tumor immune microenvironment. However, there is limited understanding of how they modulate stromal cells within the tumor microenvironment. Whether inactivating, reducing, or normalizing CAFs can decrease cancer progression and metastasis remains unclear. In this study, we investigate how artemisinin derivatives contribute to the maintenance of normalized NFs in TME. Our findings indicate that DHA and ART can significantly hinder the transformation of NFs to CAFs by blocking cancer cell-mediated PDGF-BB secretion, thereby curtailing cancer advancement. This suggests that artemisinin derivatives have the capability to disrupt the intricate interactions between tumor cells and TME.

Material and methods

Cell culture and treatment

Neutrophils were sourced from BFBCOMPETE-NTCE LL.com. (Shanghai, China). Normal human oral mucosal keratinocytes (hOMK) and normal human oral mucosal fibroblasts (hOMF) were obtained from CellResearch Corp. (Singapore). OTSCC cells (Cal-27) were obtained from BioVector (Beijing, China). The cells were cultured at 37°C and 5% CO₂ in an incubator. The cells were cultured in DMEM containing 10% FBS (Gibco), 100 U/mL penicillin, and 100 μ g/mL streptomycin (Gibco). Adherent cells were subjected to experimentation when they reached 70%-80% confluence, whereas

Antitumor effects of artemisinin derivatives

suspension cells were analyzed based on the observed formation of distinct cell clusters under a microscope. CAFs (Cal27-CM) were derived by treating hOMF with a conditioned medium from Cal-27 (Cal27-CM) at varying ratios for 48 h. CAFs (PDGF-BB) were obtained by treating the hOMF cells with PDGF-BB for 48 h.

Reagents

Antibodies against α -SMA (ab5694), PDGF-BB (ab23914), and β -tubulin (ab179513) were purchased from Abcam (Cambridge, UK). PI3K antibody (ServiceBio GB11525-50), AKT antibody (ServiceBio GB15689-50), and p-AKT antibody (ServiceBio GB150002-50) were purchased from ServiceBio. The p-PI3K antibody (Affinity AF3242) was purchased from Affinity. Recombinant human PDGF-BB was obtained from PeproTech (Beijing, China). Ki67 antibody (ServiceBio GB111499) and hematoxylin and eosin (HE) staining dye (ServiceBio G1005) were sourced from ServiceBio. Sodium oxamate (LDH-A lactate dehydrogenase inhibitor, MCE HY-W013032A) and lactate (MCE HY-B2227) were acquired from MedChemExpress (MCE). Sodium carboxymethyl cellulose (CMC-Na, MCE HY-Y1889A) and platelet-derived growth factor receptor (PDGFR) inhibitor (MCE CP73451) were also purchased from MCE. Dihydroartemisinin (Aladdin A140839-1) and artemether (Aladdin A107447-5) were obtained from Aladdin. Dimethyl sulfoxide (Solarbio D8371) was purchased from Solarbio. The MCT1/2 inhibitor was purchased from MCE (MCE AR-C155858). Pentobarbital sodium was purchased from Sigma Aldrich (Sigma Aldrich 11715-100 mg). The pan-AKT kinase inhibitor (AZD5363) was purchased from MCE (MCE HY-15431). The Akt activator (SC79) was purchased from MCE (MCE HY-18749).

Cell proliferation assay

Treatment of different cells (hOMF, Cal-27, and CAF cells) with DHA and ARM for 48 h. Afterward, CCK-8 reagent was added, and the solution was incubated for two h. The absorbance was measured using a spectrophotometer, and the cell proliferation rate was calculated from the OD value. The proliferation of Cal-27 cells in the presence of CAFs and lactic acid was assessed using the same method.

Cell apoptosis assay

Treatment of different cells (hOMF, Cal-27, and CAF cells) with DHA and ARM for 48 h. The culture supernatant was collected, and the detached cells were centrifuged at 1000 rpm for 5 min, after which the supernatant was discarded. The cells were then incubated for 20 min using the Annexin V-FITC Apoptosis Detection Kit (Beyotime Inst Biotech, China). Following incubation, apoptosis was detected using a flow cytometer (Sony ID 7000, Japan), and the apoptosis data were analyzed using FlowJo 10.9 software.

IC_{50} determination of artemisinin derivatives and cytotoxicity-free dose screening

Cal-27 and hOMF cells were treated with DHA (0, 2, 4, 8, 16, 32, 64, 128, 256, and 300 μ M) and ARM (0, 2, 4, 8, 16, 32, 64, 128, 256, and 512 μ M) for 48 h. Following this, CCK-8 reagent was added, and the solution was incubated for 2 h. The absorbance was measured using a spectrophotometer. The absorbance measurements determined the rate of cell proliferation, and dose proliferation curves for DHA and ARM in Cal-27 and hOMF cells were plotted to calculate the IC_{50} values. Based on the maximum concentration of DHA and ARM without apparent cytotoxicity, further experiments were performed to investigate their effects on Cal-27, hOMF, CAFs (Cal27-CM), and CAFs (PDGF-BB).

Cellular PDGF-BB secretion capacity assay

In a controlled assay to evaluate PDGF-BB secretion, Cal-27, hOMF, hOMK, and neutrophils were cultured at consistent densities in 6-well plates and incubated for 48 h. Clarified medium was obtained by centrifugation of the supernatant at $2000 \times g$ for 5 min, and PDGF-BB levels were determined by ELISA (RD Systems, DBB00). After DHA and ARM treatment of Cal-27 cells for 48 h, PDGF-BB levels were assayed via the method described above.

Cell morphology and spindle index

Under an OLYMPUS inverted microscope, hOMF cells subjected to diverse conditioned media were observed for morphological analysis and captured through photography. Using ImageJ software for precise measurement, the cell dimensions were recorded systematically.

Antitumor effects of artemisinin derivatives

across 3-4 randomized assessments per sample, fulfilling a count of at least 40 cells to ensure data accuracy and validity. The spindle index formula: Spindle Index = length/width (cell) [34, 35].

Analysis of cell lactate secretion capability

hOMF cells treated under various conditions were seeded in equal numbers in 6-well plates before further incubation for 48 h. Clarified medium was obtained by centrifugation of the supernatant at 2000 × g for 5 min, and lactate levels were determined using the Lactate Assay Kit (BioVision Technologies).

Western blot analysis

Proteins were extracted by lysing the cells and quantified using SDS-PAGE, followed by the transfer of the proteins to membranes (Millipore, MA, USA). The membranes were blocked with a blocking solution (Servicebio G2052) and then incubated with primary antibodies (α -SMA, PDGF-BB, Tubulin- β , 1:1000). The membranes were subsequently incubated with secondary antibodies for detection.

Transcriptome sequencing (RNA-seq)

The transcriptome sequencing (RNA-seq) in this study was performed using Cal-27 tumor cells (human origin) treated with DHA/DMSO. Total RNA was extracted from the cells using TRIzol reagent (Servicebio) after treatment. The sequencing data were analyzed by aligning to known reference genomes and annotation files. We used sequence similarity alignment to identify the expression abundance of protein-coding genes in different samples. The alignment results were obtained in counts. To eliminate the impact of differences in gene length and sequencing depth on expression quantification, we used the FPKM (Fragments Per Kilobase of transcript per Million mapped reads) method to calculate gene expression levels. Subsequently, the gene counts for each sample were normalized using DESeq2 software. Normalization was performed using the BaseMean value to estimate expression levels, and fold changes were calculated for each gene. Differential significance testing was conducted using the Negative Binomial (NB) test, and protein-coding genes with significant differential expression were identified based on fold

change and significance test results. All sequencing data have been uploaded to the GEO public database, and the data can be accessed via accession number GSE294841.

Animal source and breeding environment

The mice (BALB/c-nude) used in this study were all obtained from SPF (Beijing) Biotechnology Co., Ltd. The company's animal production license number is (SCXK-2024-0001). The mice have passed 21 parasitic and infectious disease tests, including tests for hepatitis virus, parasites, and mousepox virus. The SPF mice were housed in a standardized animal breeding environment at the Kunming Medical University Animal Laboratory. The temperature in the laboratory was controlled between 22-24°C, with humidity maintained at 40%-60%. The mice were kept on a 12 h light/12 h dark cycle, with a light intensity of approximately 200-300 lux. The mice were fed sterilized feed, and their drinking water was treated distilled water, both of which were replaced regularly. All facilities in the mouse breeding environment were thoroughly cleaned and disinfected weekly to ensure a sterile environment.

Drug safety dose screening

Animal studies were sanctioned by the Ethics Review Committee for Animal Experiments at Kunming Medical University (kmmu20230673). Four-week-old male BALB/c nude mice were selected for this experiment, acquired, and reared in a specific pathogen-free (SPF) facility. DHA and ARM were formulated into gavage-friendly emulsions using CMC-Na before administration. The study involved 21 mice divided into seven distinct groups, encompassing three mice per grouping. Over 21 days, each group was orally administered either a control solution (CMC-Na) or different dosages of DHA (50, 25, and 10 mg/kg) and ARM (75, 35, and 20 mg/kg). Body weight assessments were conducted at three-day intervals throughout the study. After completing the 21 days of treatment, mice underwent a fasting period of 12 h before being euthanized. The weights of the liver and kidneys were then recorded, and serum analyses were performed to ascertain biochemical markers of liver and kidney functionality. By evaluating growth patterns, organ weights, and liver and kidney functionality, safe drug dosages were established.

Antitumor effects of artemisinin derivatives

Tumor xenograft model

Animals were obtained and housed, as previously described. A subcutaneous Cal-27 cell xenograft mouse model was established by injecting 5×10^6 Cal-27 cells into the axillary region of mice. After six days, mice were divided into control and intervention groups. These groups underwent a daily gavage procedure for 21 uninterrupted days. Measurements were taken every third day to track changes in body weight and tumor size. On day 21, the mice were euthanized, and the final tumor weight was recorded. Moreover, a subcutaneous co-transplantation model was developed using hOMF/CAFs and Cal-27 cells. A combination of 5×10^6 hOMF/CAFs cells and 5×10^6 Cal-27 cells was injected into the axillary regions. Starting from day 6 after injection, measurements of tumor size and body mass began, followed by a regimen of daily gavage for 21 days. Every third day, we recorded the body mass and tumor dimensions. On the final day, the mice were euthanized, and tumor weights were recorded. The tumor volume was calculated using the formula: $V = 1/2 \times \text{length} \times \text{width}^2$.

Animal euthanasia

The animal experiments in this study comply with the ARRIVE guidelines. We performed euthanasia of the mice using a combination of sodium pentobarbital anesthesia and cervical dislocation. First, mice were anesthetized with an intraperitoneal injection of sodium pentobarbital (60 mg/kg), and their muscle tone, response to external stimuli, and respiratory rate were monitored to assess the anesthetic state until the mice were fully anesthetized [36]. Subsequently, the mouse's tail was grasped and swiftly pulled upward to induce cervical dislocation. Throughout the procedure, we minimized noise and ensured the operation was quick and precise to reduce the mice's stress response and minimize potential suffering.

Detection of PDGF-BB and lactate in serum from tumor-bearing mice

At the end of the animal experiments involving tumor-bearing mice, whole blood was collected from the mice. After allowing the blood to clot, the serum was separated by high-speed centrifugation ($12,000 \times g$ for 15-30 min). Serum

PDGF-BB levels and lactate concentrations were measured using a PDGF-BB ELISA kit and a lactate assay kit.

Immunohistochemistry

Tumor tissues were fixed in 4% paraformaldehyde, followed by paraffin embedding and sectioning. The section thickness was 5 μm , and the slides underwent deparaffinization and rehydration. Subsequently, tissue sections were stained using anti-Ki67 and anti- α -SMA antibodies. Hematoxylin and eosin (HE) staining was performed to observe the morphological structure of the tissue. TUNEL staining was applied to the sections to detect apoptotic cells further. Images of the stained sections were captured using an Olympus VS120 imaging system. The percentage of Ki67-positive cells was used to quantify proliferating tumor cells, while the percentage of α -SMA-positive areas was used to quantify the expression levels of α -SMA protein in the tumor tissue. The percentage of TUNEL-negative cells was used to quantify non-apoptotic cells.

Statistical analysis

Data were analyzed using GraphPad Prism 9.5. Data are presented as the mean \pm standard deviation (mean \pm SD). Data processing involved t-tests and variance analysis (ANOVA), with Bonferroni correction applied for multiple comparisons. Unless otherwise stated in the figure legend, each data point represents the average of three biological replicates. Statistical significance is interpreted as follows: $P < 0.05$ (*).

Results

PDGF-BB was upregulated and associated with poor outcomes in head and neck squamous cell carcinoma

Analysis using the online database GEPIA-2 showed that the expression of PDGF-B was significantly higher in cancer tissues (head and neck squamous cell carcinoma, HNSC) than in normal tissues. Moreover, survival was lower in patients with high expression than those with low expression (**Figure 1A, 1B**). ELISA assays of the conditioned media from different cell types showed that the PDGF-BB levels in the conditioned media of oral tongue squamous cell car-

Antitumor effects of artemisinin derivatives

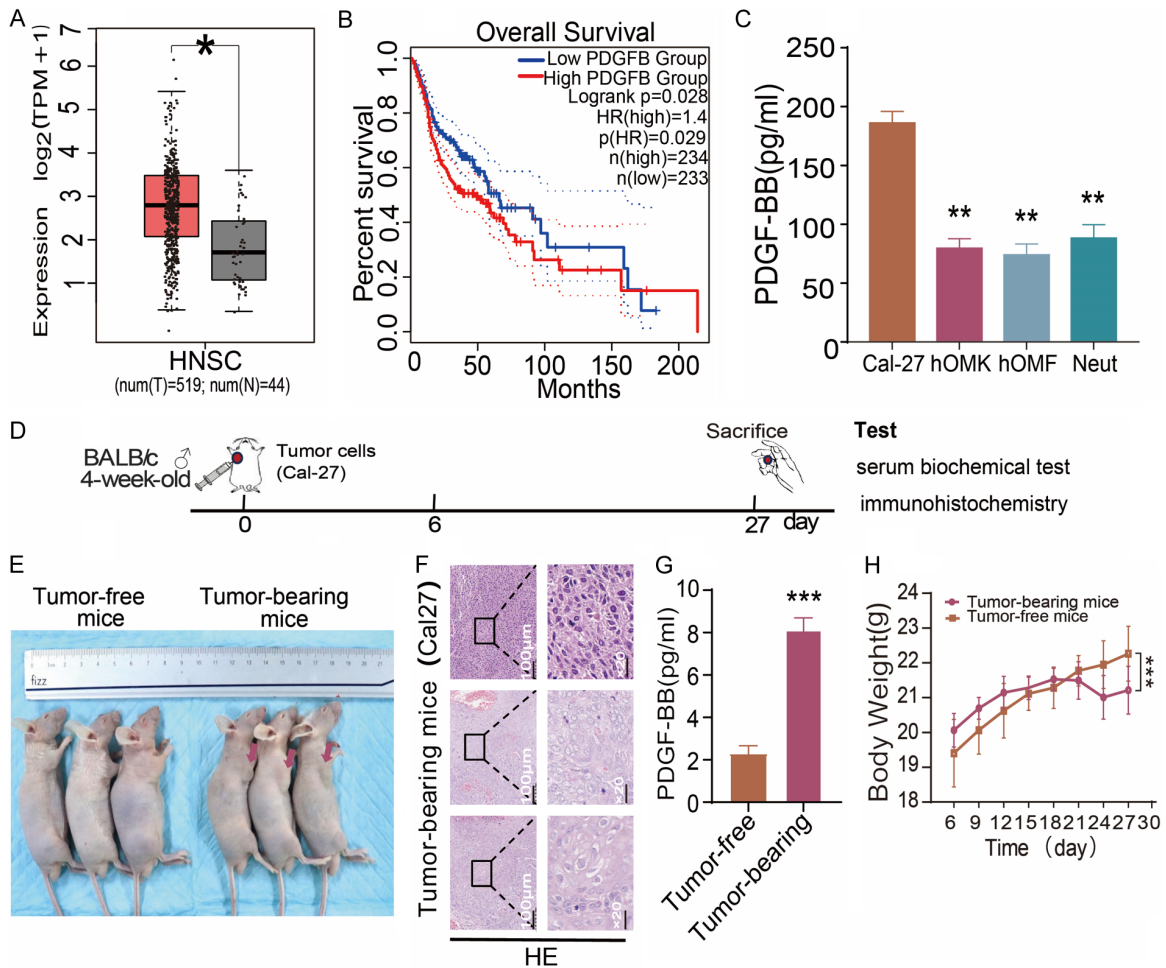


Figure 1. PDGF-B expression and Kaplan-Meier analysis of HNSC. PDGF-B expression in normal tissues and HNSC (A). Kaplan-Meier analysis of HNSC patients with high or low PDGF-B expression ($n = 467$) (B). ELISA detection of PDGF-BB expression in different cell culture media ($n = 3$) (C). Schematic diagram of experimental design of mice xenograft tumor model (D). Comparison between the tumor-bearing and tumor-free mice ($n = 3$) (E). Representative H&E staining of tumor sections from tumor-bearing mice ($n = 3$) (F). ELISA measurement of PDGF-BB expression in the sera of tumor-bearing and tumor-free mice ($n = 3$) (G). Weight changes in the tumor-bearing and tumor-free mice ($n = 3$) (H). The data were expressed as the mean \pm standard deviation (C, G, H). p values were calculated using two-sided Student's t -test ($\#P > 0.05$, $*P < 0.05$, $**P < 0.01$, $***P < 0.001$).

cinoma (OTSCC) cells (Cal-27) were significantly higher than those in oral keratinocytes (hOMK), fibroblasts (hOMF), and neutrophils (**Figure 1C**). In addition, in xenograft tumor models, we observed a significant increase in the serum levels of PDGF-BB in tumor-bearing mice and a significant decrease in the body weight of the mice (**Figure 1D-H**). Based on these findings, we concluded that PDGF-BB plays a significant role in the progression of OTSCC.

PDGF-BB induces fibroblast-to-CAF conversion to promote tumor cell proliferation

Based on our observations, OTSCC cells (Cal-27) secrete high levels of PDGF-BB (**Figure 1**).

To simulate the activation of fibroblasts by tumor-secreted products, we co-cultured hOMF cells indirectly with conditioned media (Cal27-CM) derived from Cal-27 cell supernatants at ratios of 1/4, 2/4, and 3/4 (**Figure 2A-F**). As the proportion of conditioned media increased, hOMF cells exhibited morphological changes, an increased spindle index, upregulation of α -SMA activation protein, and significantly enhanced lactate secretion (**Figure 2A-E**). These observations implied that products secreted by tumors can convert hOMF cells into CAFs (Cal-CM). The CAFs (Cal-CM) significantly enhanced the proliferation rate of Cal-27 cells (**Figure 2F**). To verify the role of PDGF-BB in the activation of fibroblasts (**Figure 2G-L**), hOMF cells were

Antitumor effects of artemisinin derivatives

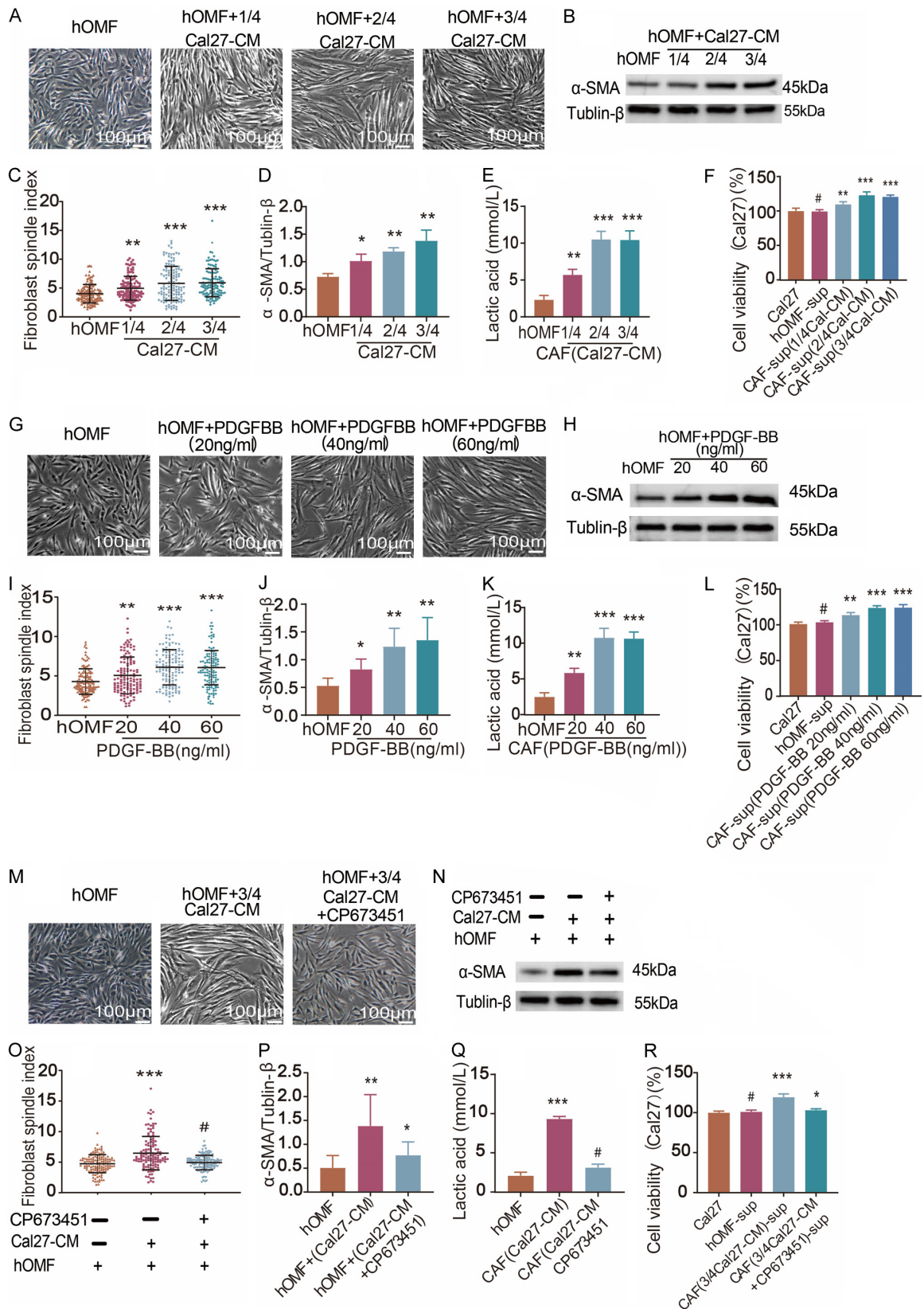


Figure 2. PDGF-BB induces fibroblast-to-CAF conversion to promote tumor cell proliferation. Evaluation of fibroblast-to-CAF conversion markers in hOMF cells treated with Cal-27 conditioned medium (Cal27-CM) at 1/4, 2/4, and 3/4 ratios for 48 h (n = 3) (A-F). Morphology of hOMF cells (Scale bar: 100 μm; n = 3) (A). Western blot analysis of α-SMA

Antitumor effects of artemisinin derivatives

protein in cells (n = 3) (B). Spindle index (n = 120) (C). Quantification of activated α -SMA protein in cells (n = 3) (D). Lactate secretion levels in CAFs (Cal27-CM) (n = 3) (E). The Effect of CAFs (Cal27-CM) on the proliferation of Cal-27 cells (n = 3) (F). Evaluation of fibroblast-to-CAF conversion markers in hOMF cells treated with 20, 40, and 60 ng/ml PDGF-BB for 48 h (n = 3) (G-L). Morphology of the hOMF cells (scale bar: 100 μ m; n = 3) (G). Western blot analysis of α -SMA protein in cells (n = 3) (H). Spindle index (n = 120) (I). Quantification of α -SMA protein in cells (n = 3) (J). Lactate secretion levels in CAFs (PDGF-BB) (n = 3) (K). Effect of CAFs (PDGF-BB) on the proliferation of Cal-27 cells (n = 3) (L). Detection of fibroblast activation markers in hOMF cells treated with a 3/4 ratio of Cal-27 conditioned medium (Cal27-CM) and PDGF-R receptor blocker (CP73451) for 48 h (n = 3) (M-R). Cell morphology (scale bar, 100 μ m; n = 3) (M). Western blot analysis of activated α -SMA in hOMF cells (n = 3) (N). Spindle index (n = 120) (O). Quantification of α -SMA protein in cells (n = 3) (P). Lactate secretion levels in the cells (n = 3) (Q). Effect of hOMF on the proliferation of Cal-27 cells (n = 3) (R). The data were expressed as the mean \pm standard deviation (C-F, I-L, O-R). *p* values were calculated using two-sided Student's *t*-test (#*P* > 0.05, **P* < 0.05, ***P* < 0.01, ****P* < 0.001).

exposed to varying PDGF-BB concentrations. The results showed that increasing PDGF-BB concentrations led to morphological changes in hOMF cells, an increased spindle index, upregulation of α -SMA activation protein, and a significant enhancement in lactate secretion (**Figure 2G-K**). The PDGF-BB-activated hOMF cells also significantly promoted the proliferation of Cal-27 cells (**Figure 2L**). Furthermore, we used the PDGF-R receptor inhibitor (CP73451). When Cal-27 cell supernatants treated with the inhibitor were used to culture hOMF cells, the activation of hOMF cells was significantly reduced (**Figure 2M-Q**). Moreover, the capacity of hOMF cells to enhance the proliferation of Cal-27 cells was considerably reduced (**Figure 2R**). The above results suggest that oral tongue squamous carcinoma cells induce fibroblast transformation to CAF by secreting PDGF-BB.

CAF-derived lactate promotes the proliferation of OTSCC cells.

In our research, we found that both the conditioned medium from Cal-27 (Cal27-CM) and PDGF-BB can trigger the conversion of hOMF cells into a CAF-like phenotype. These CAFs exhibited a marked increase in lactate production (**Figure 2**). By supplementing with lactate externally, we observed that lactate supported the proliferation of Cal-27 cells (**Figure 3E**). In the study of the role of lactate in the CAF-mediated biological behavior of tumor cells, sodium oxamate, which inhibits LDH-A, was employed to prevent CAFs from secreting lactate (**Figure 3A, 3C**). The data revealed that blocking lactate release from CAFs considerably diminished their ability to enhance the proliferation of Cal-27 cells (**Figure 3B, 3D**). To further demonstrate that the lactate derived from CAFs is a key factor in stimulating tumor cell proliferation, we treated Cal-27 cells with CAF-

conditioned medium supplemented with monocarboxylate transporter inhibitors 1 and 2 (MTCi1/2) (MTCi refers to a class of compounds that can inhibit the function of monocarboxylate transporter. These compounds work by reducing the activity of MCT, thereby blocking the transport of lactate [37-39]). The results showed that, compared to the CAF-conditioned medium alone, the CAFs-sup + MTCi group significantly inhibited Cal-27 cell proliferation (**Figure 3F, 3G**). These observations imply that lactate originating from CAFs is vital for encouraging the growth of cancer cells.

Artemisinin derivatives regulate the tumor microenvironment by targeting cancer cells in OTSCC

Based on the effects of DHA and ARM on the proliferation of Cal-27 and hOMF cells, we determined that the maximum non-inhibitory concentrations were 8 μ M for DHA and 30 μ M for ARM (**Figures 3H-M, 4C**). Furthermore, we found that at these concentrations (DHA: 8 μ M and ARM: 30 μ M), neither DHA nor ARM significantly induced apoptosis in Cal-27, hOMF, or CAF cells (**Figure 4A, 4B**) [40]. Cal-27 cells exposed to DHA (8 μ M) and ARM (30 μ M) for 48 h showed a notable reduction in PDGF-BB protein levels and secretion (**Figure 4D-F**). When we indirectly co-cultured the supernatants from DHA- and ARM-treated Cal-27 cells with hOMF cells, there was a considerable reduction in the spindle-shaped index of hOMF cells, a decline in the activation marker α -SMA, as well as decreased lactate secretion and reduced growth impact on Cal-27 cells (**Figure 4G-L**). We also investigated the implications of DHA and ARM on CAFs, revealing that these compounds did not substantially alter CAF activation markers (**Figure 5A-E**). Administering DHA or ARM to CAFs showed no notable

Antitumor effects of artemisinin derivatives

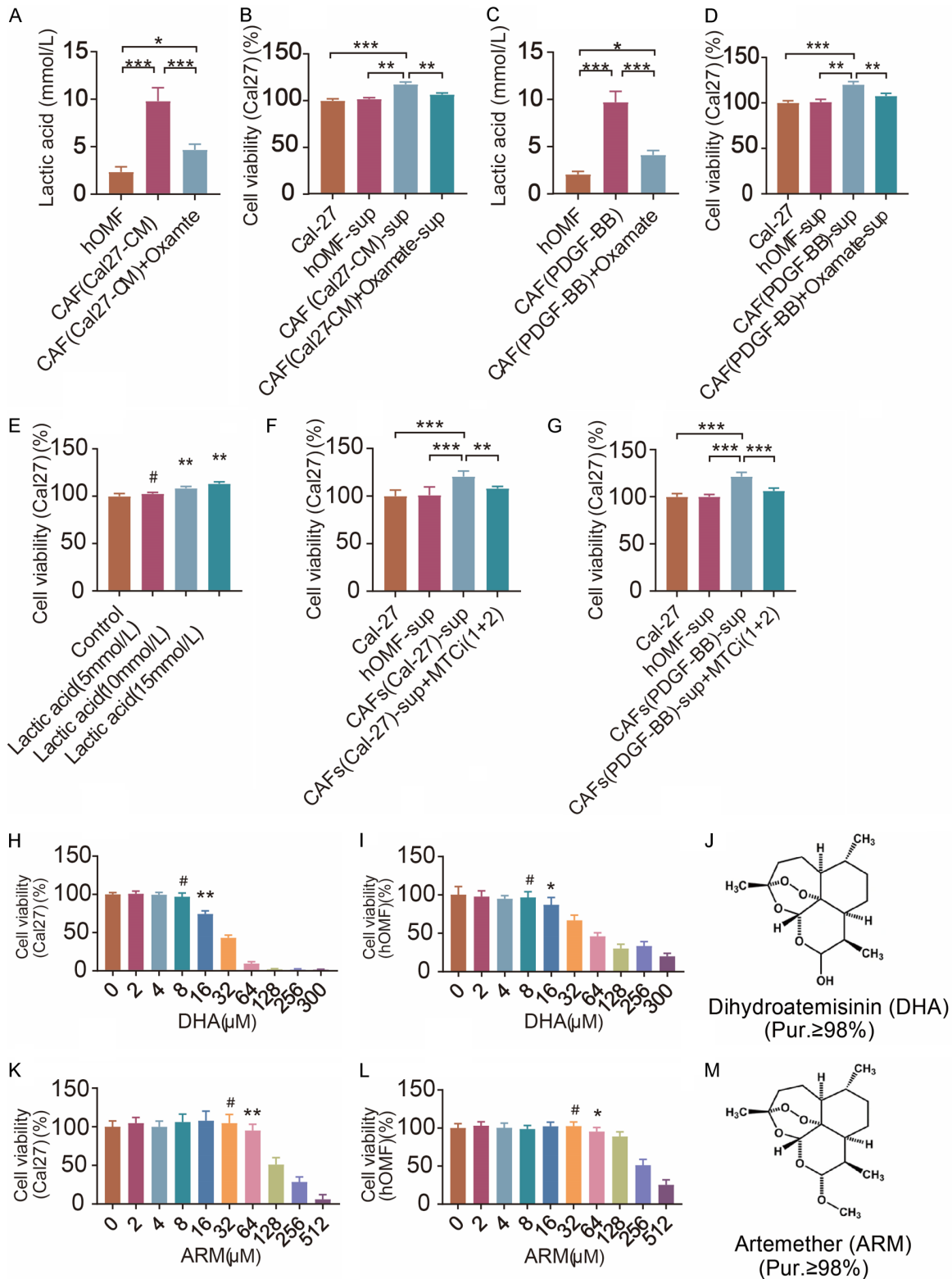


Figure 3. Lactate from CAFs promotes the proliferation of Cal-27 cells and the inhibitory concentration of artemisinin derivatives on hOMF and Cal-27 cells. Lactate secretion levels in CAFs (Cal27-CM) treated with NaOx for 48 h (n = 3) (A). The effect of sodium oxalate-treated CAFs (Cal27-CM) on the proliferation of Cal-27 cells (n = 3) (B). Lactate secretion levels in CAFs (PDGF-BB) treated with NaOx for 48 h (n = 3) (C). Effect of sodium oxalate-treated CAFs (PDGF-BB) on the proliferation of Cal-27 cells (n = 3) (D). Proliferation of Cal-27 cells treated with 5, 10, and 15 mmol/L lactate (n = 3) (E). Proliferation of Cal-27 cells after adding monocarboxylate transporter (MCT) inhibitors 1

Antitumor effects of artemisinin derivatives

and 2 to CAFs (Cal27-CM)-conditioned medium (n = 3) (F). Proliferation of Cal-27 cells after adding monocarboxylate transporter (MCT) inhibitors 1 and 2 to CAFs (PDGF-BB)-conditioned medium (n = 3) (G). Effect of DHA on the proliferation of Cal-27 (H) and hOMF cells (I) at concentrations of 0, 2, 4, 8, 16, 32, 64, 128, 256, and 300 μM (n = 3) (H, I). Effect of ARM on the proliferation of Cal-27 (K) and hOMF cells (L) at concentrations of 0, 2, 4, 8, 16, 32, 64, 128, 256, 512, and 600 μM (n = 3) (K, L). Chemical structures and purity of DHA and ARM, with purity of DHA and ARM greater than or equal to 98% (J, M). The data were expressed as the mean \pm standard deviation (A-I, K, L). p values were calculated using two-sided Student's t-test (#P > 0.05, *P < 0.05, **P < 0.01, ***P < 0.001).

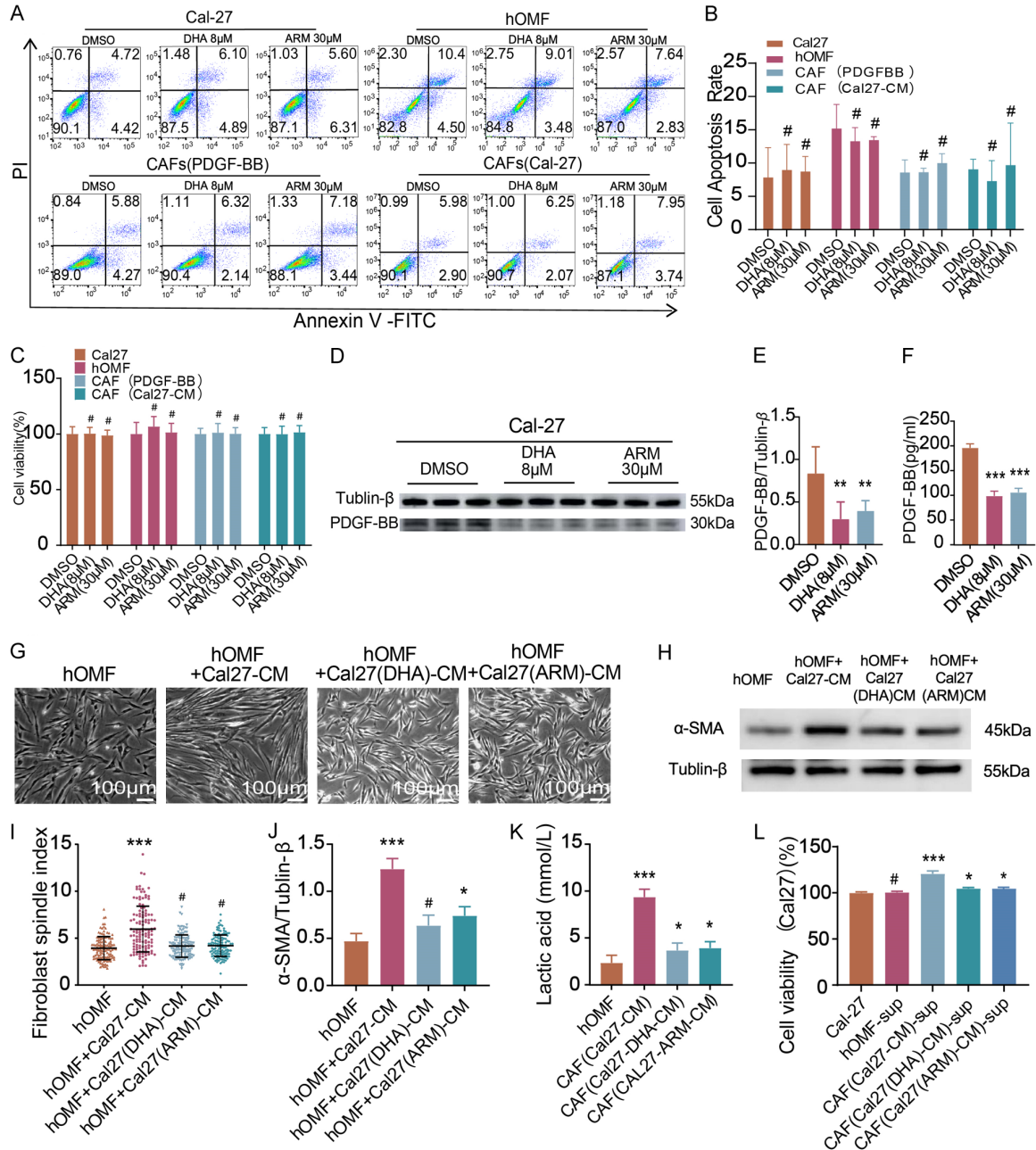


Figure 4. Artemisinin derivatives inhibit the secretion of PDGF-BB by Cal-27 cells, reducing the transformation of hOMF into CAF. Apoptosis results of flow cytometry (n = 3) (A). Apoptosis statistics (n = 3) (B). Effect of DHA (8 μM) and ARM (30 μM) on the proliferation of Cal-27, hOMF, CAFs (Cal27-CM), and CAFs (PDGF-BB) (n = 3) (C). Intracellular expression and quantification of PDGF-BB in Cal-27 cells treated with DHA or ARM (n = 3) (D, E). ELISA analysis of PDGF-BB expression levels in Cal-27 cells treated with DHA and ARM (n = 3) (F). Analysis of hOMF cell activation markers following 48-h treatment with Cal-27 (DHA/ARM)-conditioned medium (G-L). Morphology of the hOMF cells (scale bar: 100 μm ; n = 3) (G). Western blotting analysis of α -SMA protein expression (n = 3) (H). Spindle index (n

Antitumor effects of artemisinin derivatives

= 120) (I). Quantification of α -SMA protein expression (n = 3) (J). Lactate secretion in hOMF cells (n = 3) (K). Effect of hOMF on the proliferation of Cal-27 cells (n = 3) (L). The data were expressed as the mean \pm standard deviation (B, C, E, F, I-L). *p* values were calculated using two-sided Student's *t*-test (#*P* > 0.05, **P* < 0.05, ***P* < 0.01, ****P* < 0.001).

change in their influence on the proliferation of Cal-27 cells (**Figure 5F**). Additionally, while exploring DHA and ARM as potential inhibitors of PDGF-BB-induced hOMF activation, we found that despite DHA (8 μ M) and ARM (30 μ M) reducing the transformation markers associated with PDGF-BB-induced conversion of hOMF to CAFs (**Figure 5G-K**), these CAFs did not significantly reduce Cal-27 cell proliferation (**Figure 5L**). These outcomes imply that artemisinin derivatives help normalize hOMF by primarily targeting oral tongue squamous carcinoma (OTSCC) cells to reduce PDGF-BB secretion.

Artemisinin derivatives target the PI3K-AKT signaling pathway to inhibit tumor cell PDGF-BB expression

This study found that artemisinin derivatives can effectively inhibit the secretion of PDGF-BB and suppress its expression in tumor cells (**Figure 4**), providing further insight into their mechanism of action. We selected tumor cells treated with DHA for transcriptome sequencing, and the results showed that 242 genes were downregulated (*P* < 0.05, Log₁₀ FC < -1) (**Figure 6A**). Further pathway enrichment analysis using WIKI and KEGG showed that both pathways were enriched in the PI3K-AKT pathway (**Figure 6B, 6C**). Western blotting revealed that after DHA and ARM treatment, the expression of p-PI3K and p-AKT was significantly downregulated (**Figure 6D-G**). When tumor cells were treated with the AKT inhibitor (AZD5363), PDGF-BB expression was downregulated considerably (**Figure 6H-J**). To further verify the relationship between this pathway and PDGF-BB, we utilized an AKT activator (SC79), which led to a significant upregulation of PDGF-BB. Additionally, co-treatment with the AKT activator and DHA/ARM caused a downregulation of PDGF-BB expression in tumor cells (**Figure 6K-M**). These results suggest that artemisinin derivatives can inhibit tumor cell PDGF-BB expression by targeting the PI3K-AKT pathway.

Artemisinin derivatives effectively inhibit tumor progression at safe doses

DHA and ARM are derivatives of artemisinin, which, as first-line antimalarial drugs, have

been widely recognized for their safety [23]. However, the drug concentrations and treatment durations used in antitumor therapies differ significantly from those used in antimalarial treatments [41]. First, we screened for safe doses of DHA and ARM to assess the safety and antitumor efficacy of artemisinin derivatives in cancer therapy. The mice were categorized into three dose groups (high, medium, and low dose groups), and the CMC-Na group (high dose: DHA 50 mg/kg, ARM 75 mg/kg; medium dose: DHA 25 mg/kg, ARM 35 mg/kg; low dose: DHA 10 mg/kg, ARM 20 mg/kg; control group: CMC-Na) for 21 consecutive days (**Figure 7A**). The results revealed that, in the high-dose group, the mice's body, liver, and kidney weights significantly decreased (**Figure 7B-D**). Further biochemical analysis of liver and kidney functions indicated varying degrees of damage in the high-dose group (**Figure 7E-I**). In the medium-dose group, only a few parameters showed changes (**Figure 7B-I**). In the low-dose group, no significant differences were observed in physiological functions compared with the control group (**Figure 7B-I**). These findings established a medium dose (DHA, 25 mg/kg; ARM, 35 mg/kg) as the maximum safe dose. Subsequently, medium and low doses were administered to the tumor-bearing mice (Cal-27 model). At medium doses of DHA and ARM, tumor (Cal-27 model) proliferation was significantly inhibited, whereas no significant inhibitory effect was observed at the low dose (**Figure 7K-P**). These results suggest that when administered within a long-term, safe dosage range, artemisinin derivatives can effectively inhibit tumor proliferation.

Fibroblast-to-CAFs transition promotes the progression of OTSCC

To explore the impact of CAFs on OTSCC progression and determine if OTSCC can transform hOMF into CAFs, we developed a tumor model with both hOMF/CAFs and Cal-27 tumor cells implanted together (**Figure 8A**). The findings indicated that the tumor size in the group where CAFs and Cal-27 were co-implanted was considerably larger than in the group with only Cal-27 (**Figure 8B-J**). Additionally, beginning on day

Antitumor effects of artemisinin derivatives

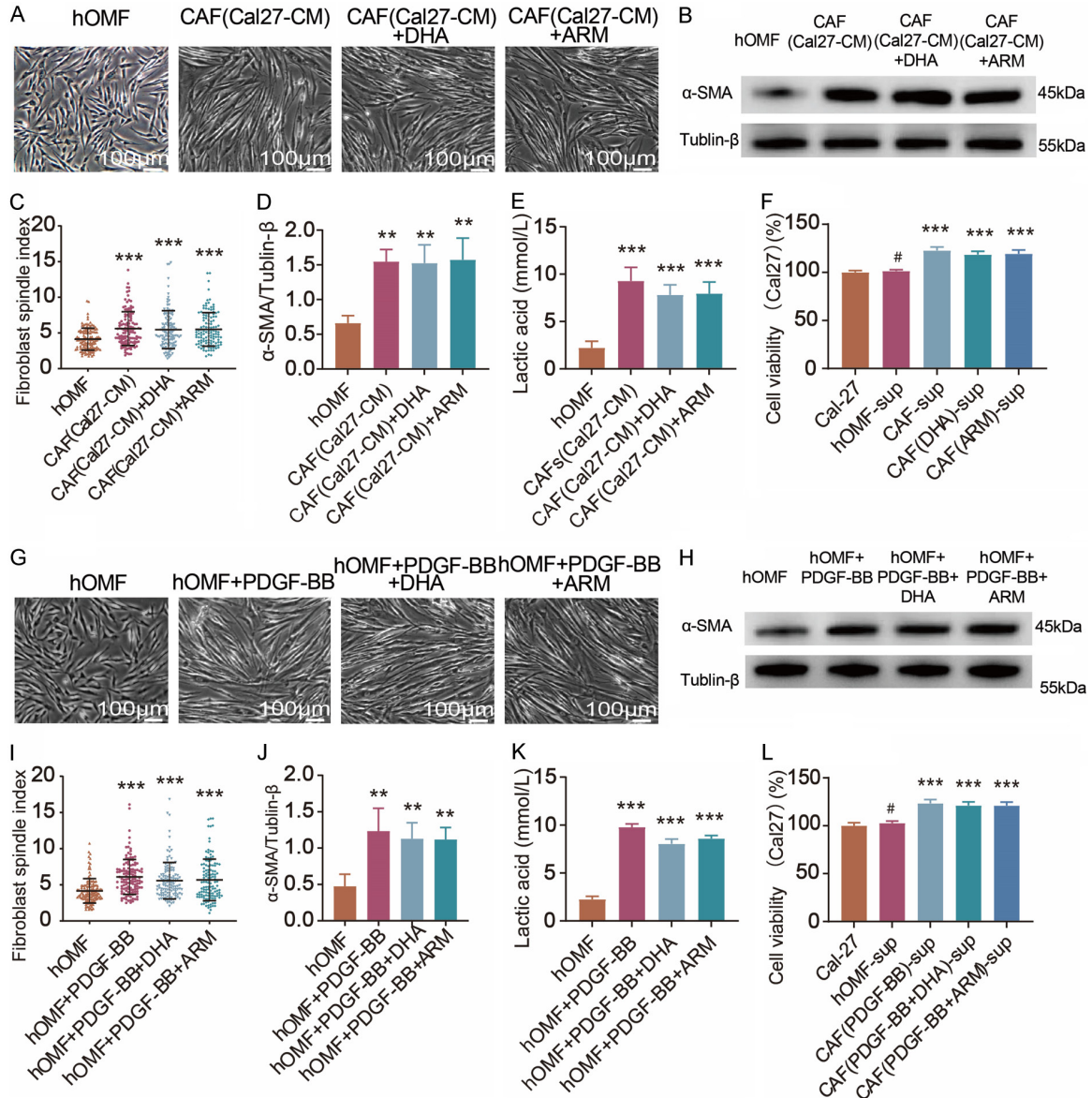


Figure 5. Artemisinin derivatives have a limited effect on reversing CAF function and blocking PDGF-BB activation pathways. After 48 h treatment of CAFs (Cal27-CM) with DHA (8 μM) and ARM (30 μM), related CAFs markers were assessed (n = 3) (A-F). Morphology of the CAF cells (scale bar: 100 μm; n = 3) (A). Western blot analysis of α-SMA protein expression in CAF (n = 3) (B). Spindle cell index of CAF (n = 120) (C). Quantifying activated α-SMA protein expression in CAF cells (n = 3) (D). Lactate secretion in CAFs cells (n = 3) (E). Effect of CAF on proliferation of Cal-27 cells (n = 3) (F). After co-treatment of hOMF cells with PDGF-BB and DHA or ARM, the related activation markers in hOMF cells were assessed (n = 3) (G-L). Morphology of the hOMF cells (scale bar: 100 μm; n = 3) (G). Western blotting analysis of α-SMA protein expression in hOMF cells (n = 3) (H). Spindle cell index of hOMF cells (n = 120) (I). Quantification of α-SMA expression in hOMF cells (n = 3) (J). Lactate secretion in hOMF cells (n = 3) (K). Effect of hOMF on the proliferation of Cal-27 cells (n = 3) (L). The data were expressed as the mean ± standard deviation (C-F, I-L). *p* values were calculated using two-sided Student's *t*-test (#*P* > 0.05, **P* < 0.05, ***P* < 0.01, ****P* < 0.001).

15 after implantation, a clear difference in tumor size emerged between groups co-implanted with hOMF/Cal-27 and those with just Cal-27 (Figure 8C). Moreover, lactate concentrations were significantly elevated in the

co-implanted groups compared to the Cal-27-only group (Figure 8G). Immunohistochemistry showed substantially higher α-SMA expression in the hOMF/Cal-27 co-implantation group relative to the Cal-27-only group. The fraction of

Antitumor effects of artemisinin derivatives

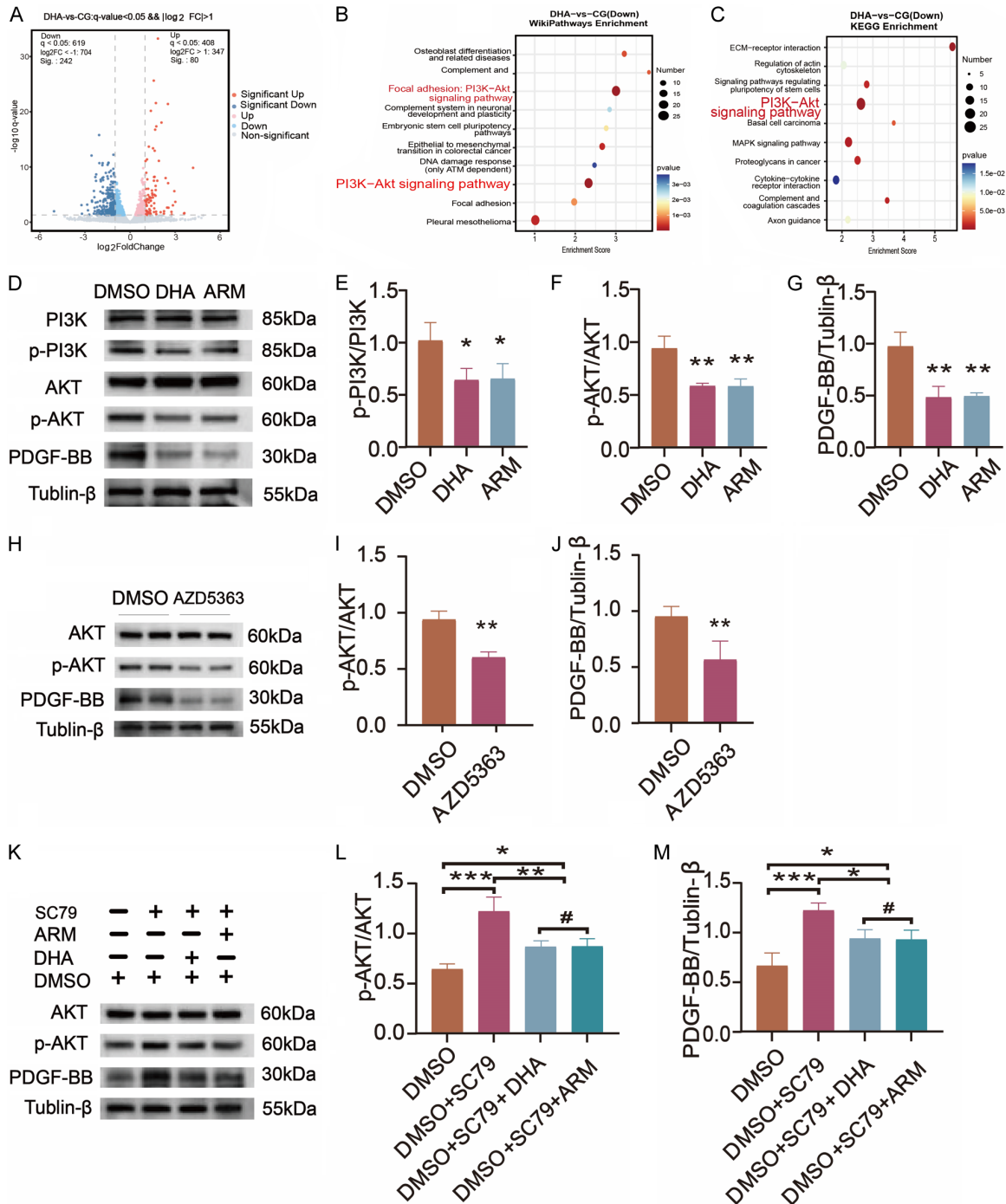


Figure 6. Artemisinin derivatives interfere with the PI3K-AKT pathway to inhibit tumor cell PDGF-BB expression. Transcriptomic data analysis after DHA (8 μM) treatment of tumor cells for 48 hours (n = 3) (A-C). Volcano plot of differentially expressed genes (P < 0.05, Log₁₀ FC < -1) (n = 3) (A). WikiPathway enrichment (n = 3) (B). KEGG pathway enrichment (n = 3) (C). Western blotting and quantification results of PI3K-AKT proteins after DHA and ARM treatment of tumor cells (n = 3) (D-G). Western blot of PI3K, p-PI3K, AKT, p-AKT, and PDGF-BB after DHA and ARM treatment of tumor cells (n = 3) (D). Quantification of p-PI3K/PI3K (n = 3) (E). Quantification of p-AKT/AKT (n = 3) (F). Quantification of PDGF-BB (n = 3) (G). Expression of p-AKT, AKT, and PDGF-BB after AKT inhibitor (AZD5363) treatment of tumor cells (n = 3) (H-J). Western blot of p-AKT, AKT, and PDGF-BB after AKT inhibitor (AZD5363) treatment of tumor cells (n = 3) (H). Quantification of p-AKT/AKT (n = 3) (I). Quantification of PDGF-BB (n = 3) (J). Expression of p-AKT, AKT, and PDGF-BB after AKT activator (SC79)/DHA and ARM treatment of tumor cells (n = 3) (K-M). Western blot of p-AKT, AKT, and PDGF-BB after AKT activator (SC79)/DHA and ARM treatment of tumor cells (n = 3) (K). Quantification of p-AKT/AKT (n = 3) (L). Quantification of PDGF-BB (n = 3) (M). p values were calculated using two-sided Student's t-test (#P > 0.05, *P < 0.05, **P < 0.01, ***P < 0.001).

Antitumor effects of artemisinin derivatives

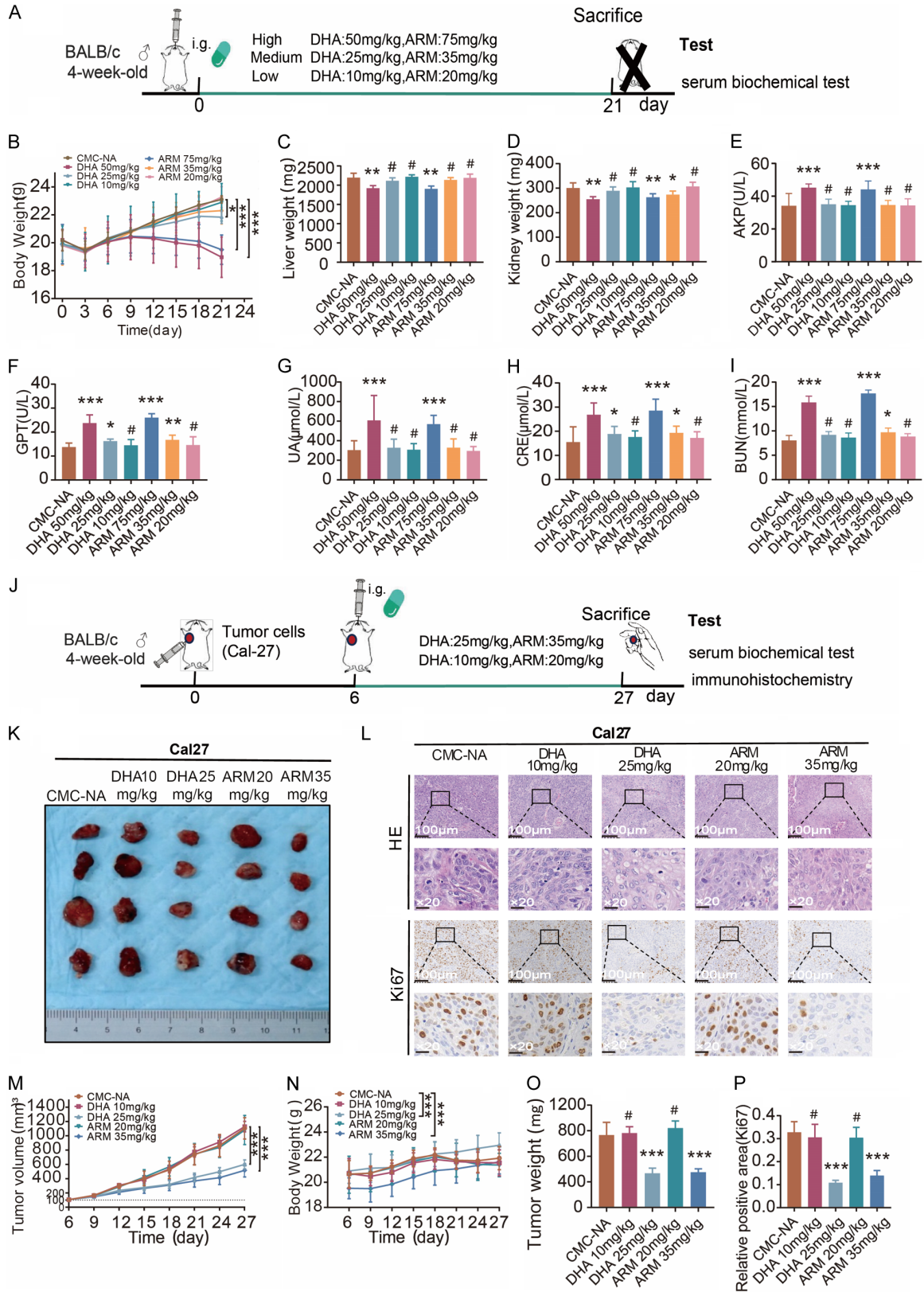


Figure 7. Artemisinin derivative safety dose screening and antitumor effects. Mice were administered DHA (50, 25, and 10 mg/kg), ARM (75, 35, and 20 mg/kg), and CMC-NA via gavage daily. Body weight was measured every three days until the end of the experiment, and mouse serum was collected to assess liver and kidney function-related

Antitumor effects of artemisinin derivatives

biochemical parameters (n = 3) (B-I). Schematic diagram of the experimental design for safe dose screening of DHA and ARM in mice (A). Body weight change in mice (n = 3) (B). Liver weights of mice (n = 3) (C). Kidney weight of mice (n = 3) (D). Serum alkaline phosphatase (AKP) level (n = 3) (E). Serum alanine aminotransferase (GPT) levels (n = 3) (F). Serum uric acid (UA) level (n = 3) (G). Serum blood urea nitrogen (CRE) levels (n = 3) (H). Serum creatinine (BUN) level (n = 3) (I). Tumor-bearing mice (Cal-27 model) were gavaged daily with DHA (25 and 10 mg/kg), ARM (35 and 20 mg/kg), and CMC-Na, and body weight and tumor size were measured every 3 days until the end of the experiment (n = 4) (J-P). Schematic diagram of the experimental design for DHA and ARM treatment in tumor-bearing (Cal-27) mice (J). Tumor images (K). Representative histological images of tumor sections stained with hematoxylin and Eosin (HE) and Ki67 immunohistochemistry (IHC) (scale bar: 100 μ m; n = 4) (L). Graph of changes in tumor size (n = 4) (M). Graph showing changes in mouse body weight (n = 4) (N). Tumor weight (n = 4) (O). Proportion of Ki67 immunohistochemically positive cells in tumor sections (n = 4) (P). The data were expressed as the mean \pm standard deviation (B-I, M-P). *p* values were calculated using two-sided Student's t-test (#*P* > 0.05, **P* < 0.05, ***P* < 0.01, ****P* < 0.001).

Ki67-positive cells also increased significantly (**Figure 8E, 8H, 8I**). Additionally, no significant TUNEL-positive apoptotic cells were observed (**Figure 8E, 8J**). These results collectively suggest that fibroblasts (hOMF) and CAFs do not induce apoptosis in tumor cells *in vivo*. On the contrary, CAFs play an active role in promoting tumor progression, particularly after hOMF are converted into CAFs in the tumor microenvironment, enhancing tumor growth by releasing lactate.

Artemisinin derivatives as potential targeted therapies for disrupting tumor-stroma interactions in the OSTCC

To clarify the impact of artemisinin derivatives on modifying the tumor microenvironment (TME), we noted that small doses of DHA and ARM (10 mg/kg and 20 mg/kg) showed no substantial inhibitory effects on tumor growth (Cal-27 model) when compared to the control group (CMC-Na) (**Figure 7J-P**). Testing these concentrations in the tumor model (Cal-27) affirmed these consistent findings, with no notable alterations in tumor size (**Figure 9A-D, 9F**). Immunohistochemical evaluation of the tumor samples revealed no significant difference in the ratio of Ki67-positive cells between the groups treated and the control (CNC-Na) (**Figure 9E, 9H**). Further analysis using TUNEL staining showed that there was no effective induction of apoptosis in tumor cells *in vivo* at this concentration (**Figure 9E, 9I**). However, at these doses, the level of PDGF-BB in the serum of treated mice was significantly reduced, indicating that DHA and ARM altered the tumor's secretion behavior *in vivo* (**Figure 9G**). In the drug sensitivity experiments, the IC_{50} values for DHA on Cal-27 cells and hOMF were 27.14 μ M and 71.95 μ M, respectively, while for ARM, these values were 151.6 μ M and 284.8 μ M

(**Figure 9J, 9K**). These findings reveal that hOMF cells demonstrate a notably reduced sensitivity to DHA and ARM compared to Cal-27 cells. Therefore, when doses of DHA and ARM at 10 and 20 mg/kg were administered, there was no observed effect on hOMF cell proliferation in tumors co-transplanted with Cal-27. We investigated the antitumor mechanisms of artemisinin derivatives at these low levels by constructing a co-transplantation model combining hOMF with Cal-27. This study showed that DHA and ARM notably impeded tumor progression at doses of 10 mg/kg and 20 mg/kg (**Figure 10A-D, 10F**). The tumors displayed a pronounced decrease in serum PDGF-BB levels among the mice bearing tumors (**Figure 10J**). Immunohistochemical analyses indicated a marked downregulation of α -SMA and reduced counts of Ki67-positive cells (**Figure 10E, 10G, 10H**). TUNEL staining showed no significant positive cells (**Figure 10E, 10I**). Furthermore, mice in the treatment groups showed significantly lower serum lactate levels (**Figure 10K**). These outcomes imply that artemisinin derivatives impede tumor development by interfering with interactions between cancer cells and stromal components.

Discussion

PDGF-BB, an important component of the PDGF family, is elevated in numerous cancer types and is intricately linked with cell growth, invasion, and cancer spread [16]. In non-small cell lung cancer (NSCLC), both PDGF-BB and PDGF-R- α are highly expressed and linked to poor prognosis [42]. Our research verified the link between high PDGF-BB expression and unfavorable outcomes in HNSC patients. The PDGF-BB/PDGF-R β signaling pathway induces the transformation of pericytes into CAFs and

Antitumor effects of artemisinin derivatives

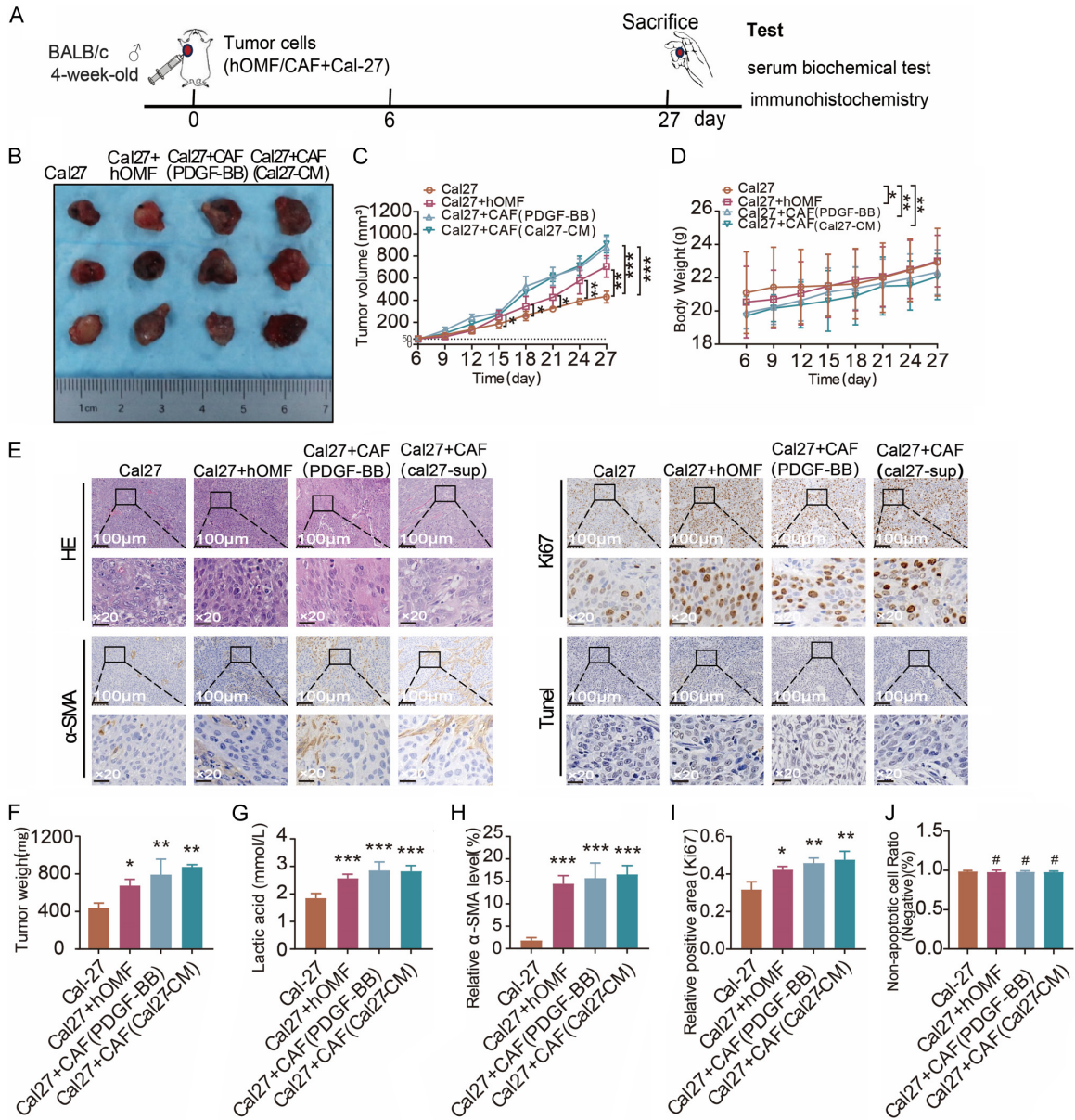


Figure 8. CAFs promote the progression of oral squamous cell carcinoma. Schematic diagram of the experimental design for co-transplantation hOMF/CAFs with Cal-27 in tumor-bearing mice (A). Tumor pictures (n = 4) (B). Graph of changes in tumor size (n = 4) (C). Graph of changes in mouse body weight (n = 4) (D). Representative histological images of tumor sections (hOMF/Cal-27) stained with hematoxylin and eosin (HE), α -SMA, Ki67, and TUNEL (scale bar: 100 μ m; n = 4) (E). Tumor weight (n = 4) (F). Serum lactate levels in the tumor-bearing mice (n = 4) (G). Proportion of α -SMA immunohistochemical staining in tumor sections (n = 4) (H). Proportion of Ki67 immunohistochemically positive cells in tumor sections (n = 4) (I). The proportion of TUNEL negative cells in tumor sections (n = 4) (J). The data are expressed as mean \pm standard deviation (C, D, F-J). P values were calculated using a two-sided Student's t-test (#P > 0.05, *P < 0.05, **P < 0.01, ***P < 0.001).

promotes tumor invasion and metastasis [43]. We found that CAFs can originate from NFs, which are directly activated by PDGF-BB secreted by tumor cells, acquiring a characteristic CAF phenotype (e.g., upregulation of α -SMA, changes in cell morphology, and altered secre-

tory functions). The altered secretory function of CAFs directly leads to increased lactate production. Further experiments demonstrated that fibroblasts treated with PDGF-BB- or Cal-27-conditioned media produced supernatants and lactate, which significantly enhanced the

Antitumor effects of artemisinin derivatives

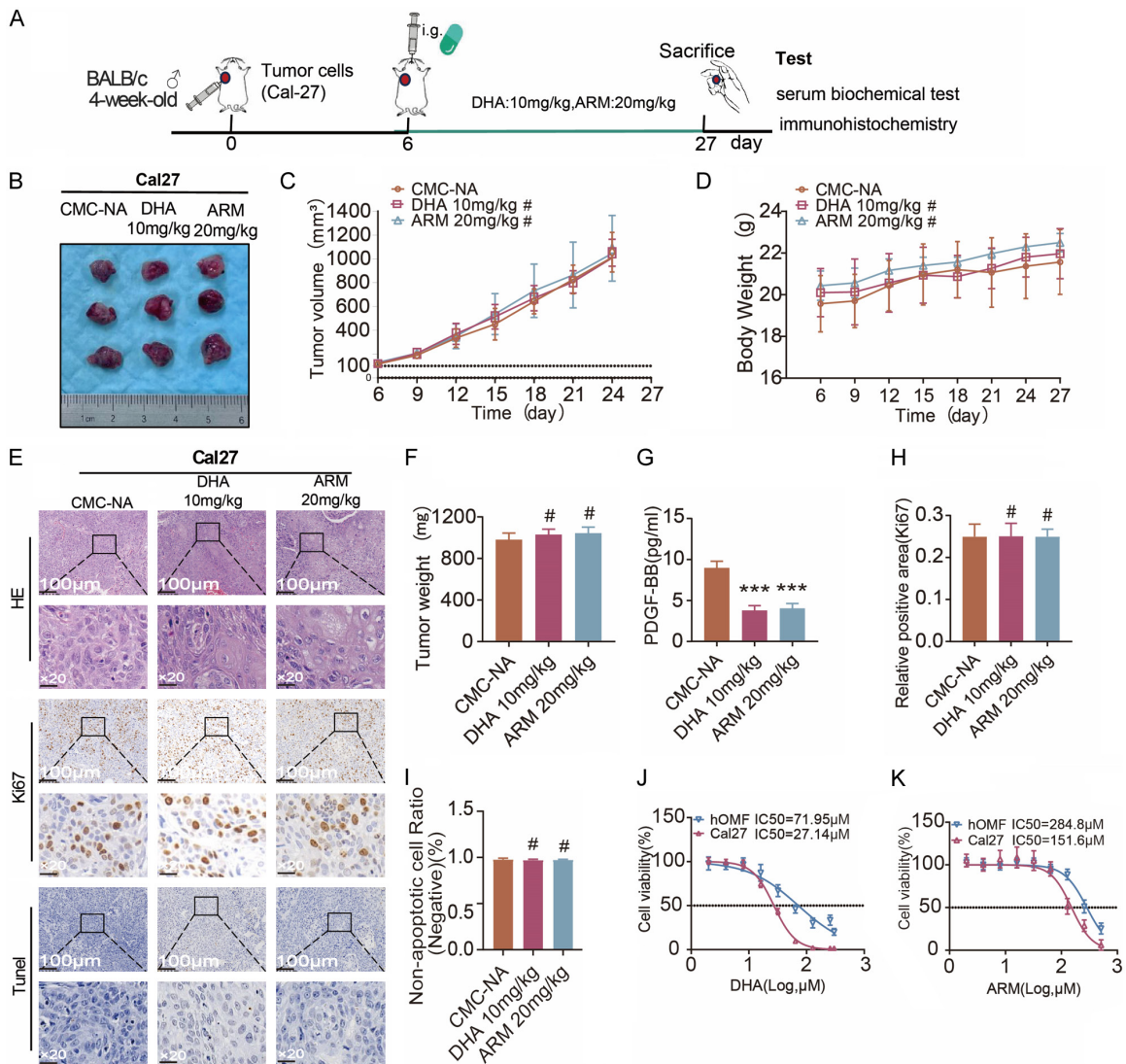


Figure 9. Artemisinin derivatives inhibit tumor secretion in vivo. Tumor-bearing (Cal-27) mice were orally administered DHA (10 mg/kg) and ARM (20 mg/kg) daily. Mouse body weight and tumor size were measured every three days until the end of the experiment ($n = 3$). Schematic diagram of the experimental design for DHA and ARM treatments in tumor-bearing (Cal-27) mice (A). Images of tumors (Cal-27) ($n = 3$) (B). Graph of changes in tumor size (Cal-27) ($n = 3$) (C). Graph of changes in mouse body weight (Cal-27) ($n = 3$) (D). Representative histological images of tumor sections (Cal-27) stained with hematoxylin and eosin (HE), Ki67, and TUNEL (scale bar: 100 μm ; $n = 3$) (E). Tumor weight (Cal-27) ($n = 3$) (F). ELISA measurement of PDGF-BB levels in the serum of tumor-bearing mice ($n = 3$) (G). Proportion of Ki67 immunohistochemically positive cells in tumor sections ($n = 3$) (H). The proportion of TUNEL negative cells in tumor sections ($n = 3$) (I). Dose-response curves for DHA on Cal-27 and hOMF cell proliferation with IC_{50} values ($n = 3$) (J). Dose-response curves for ARM on Cal-27 and hOMF cell proliferation with IC_{50} values ($n = 3$) (K). The data were expressed as the mean \pm standard deviation (C, D, F-K). P values were calculated using a two-sided Student's t -test (# $P > 0.05$, * $P < 0.05$, ** $P < 0.01$, *** $P < 0.001$).

proliferative capacity of Cal-27 cells. Notably, unlike immune cells, normal fibroblasts do not possess the ability to kill tumor cells directly. However, when fibroblasts are reprogrammed by the tumor microenvironment and acquire cancer-associated features, they participate in

tumor growth and metastasis [44]. Our experiment found that hOMF did not significantly promote tumor proliferation or induce apoptosis in tumor cells. Compared to CAFs (cancer-associated fibroblasts), normal fibroblasts have weaker tumor-promoting effects. In other words, nor-

Antitumor effects of artemisinin derivatives

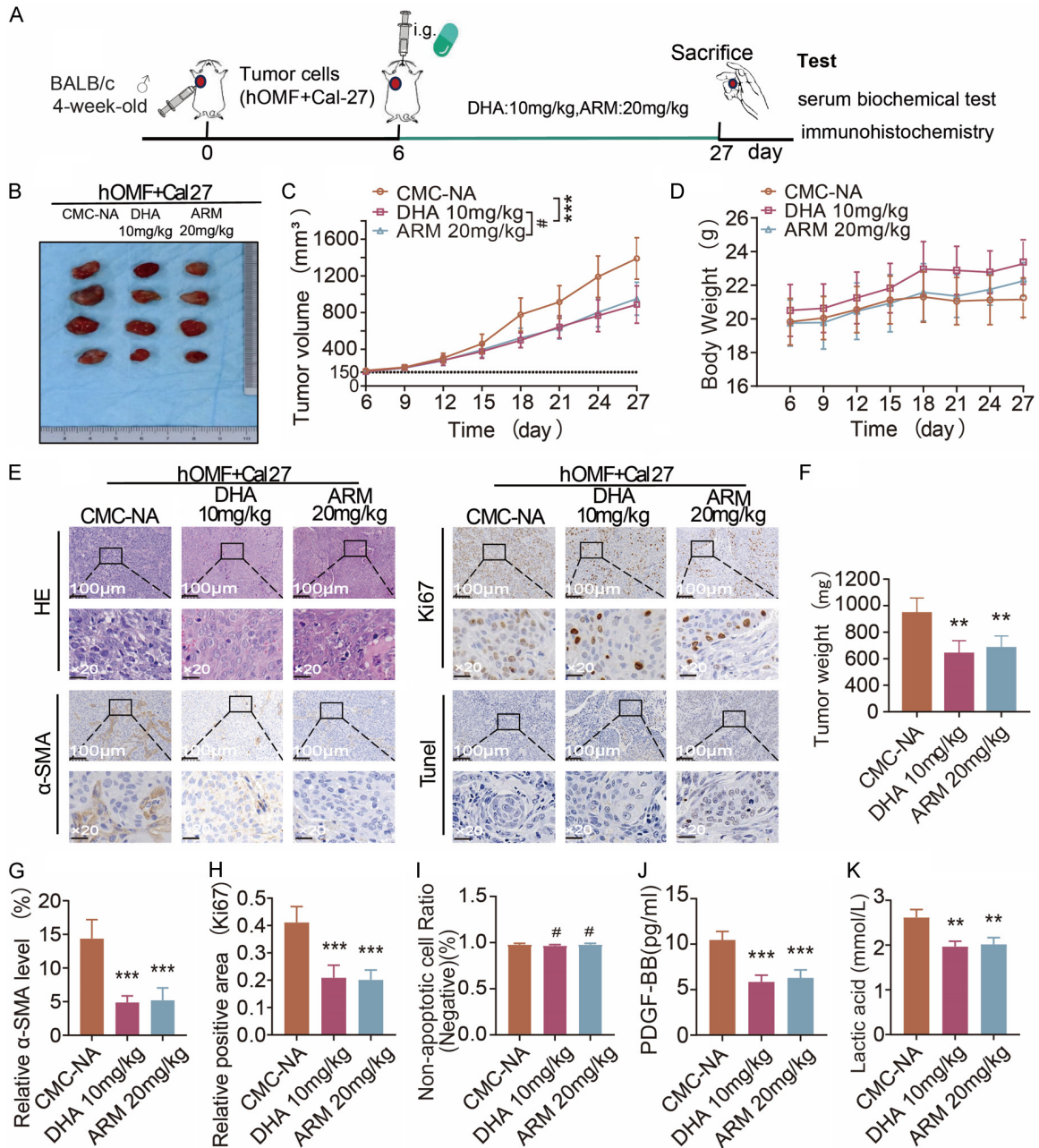


Figure 10. Artemisinin derivatives are potential targeted drugs for interfering with tumor-stroma therapy in OSTCC. hOMF/Cal-27 co-implanted tumor-bearing mice were orally administered DHA (10 mg/kg) and ARM (20 mg/kg) daily. Mouse body weight and tumor size were measured every three days until the end of the experiment (n = 4). Schematic diagram of the experimental design for DHA and ARM treatment in hOMF/Cal-27 co-implanted tumor-bearing mice (A). Tumor pictures (hOMF/Cal-27) (n = 4) (B). Graph of changes in tumor size (hOMF/Cal-27) (n = 4) (C). Graph of changes in mouse body weight (n = 4) (D). Representative histological images of tumor sections (hOMF/Cal-27) stained with hematoxylin and eosin (HE), α -SMA, Ki67, and TUNEL (scale bar: 100 μ m; n = 4) (E). Tumor weights of the mice (n = 4) (F). The proportion of α -SMA-positive cells in tumor sections (hOMF/Cal-27) by immunohistochemistry (n = 4) (G). Proportion of Ki67-positive cells in tumor sections (hOMF/Cal-27) by immunohistochemistry (n = 4) (H). The proportion of TUNEL negative cells in tumor sections (n = 4) (I). ELISA measurement of PDGF-BB levels in the sera of tumor-bearing mice (n = 4) (J). Serum lactate levels in the tumor-bearing (hOMF/Cal-27) mice (n = 4) (K). The data were expressed as the mean \pm standard deviation (C, D, F-K). P values were calculated using two-sided Student's t-test (#P > 0.05, *P < 0.05, **P < 0.01, ***P < 0.001).

mal fibroblasts might remain neutral in influencing tumor cell biological behavior [45-48].

This provides a theoretical basis for targeting CAF generation to offer anti-tumor strategies.

Antitumor effects of artemisinin derivatives

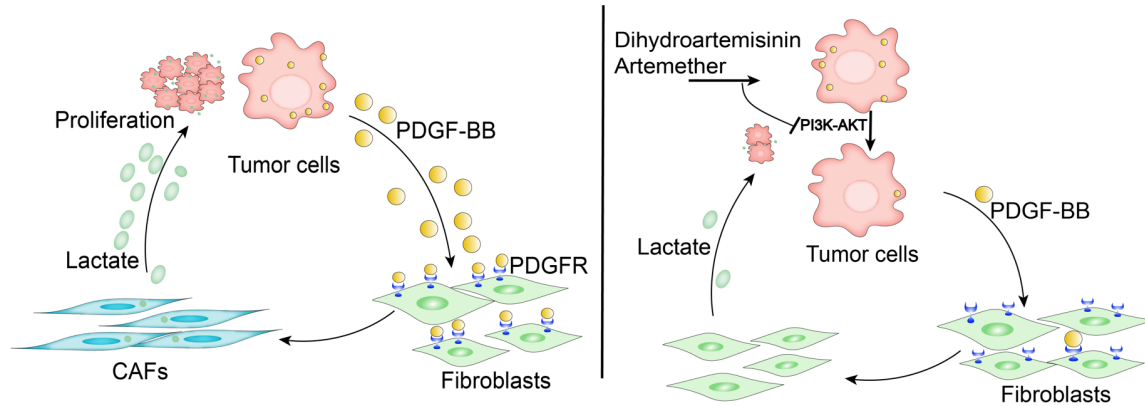


Figure 11. Artemisinin derivatives maintain fibroblast normalization by targeting tumor cells (Graphical abstract).

As a critical component of the tumor stroma, CAF promotes the formation of complex network systems in the tumor microenvironment, which further contributes to tumor invasion and metastasis [9]. Although CAF plays a crucial potential role in cancer therapy, targeted therapy against CAF in the clinic still faces numerous challenges. Current treatment strategies include reducing the number of CAFs, normalizing CAFs, and preventing their production [49, 50]. However, despite the development of drugs targeting CAFs based on these strategies, issues such as side effects and poor targeting specificity present limitations [51, 52]. Research has demonstrated that artemisinin derivatives exhibit antitumor effects and can block PDGFR/ERK-induced pulmonary fibrosis [22, 53]. In fibrotic diseases, the matrix released by fibroblasts does not independently block fibrosis, and the transformation of fibroblasts into CAFs in the tumor microenvironment is mainly irreversible [9, 54]. Therefore, exploring the interference of artemisinin derivatives in fibroblast-to-CAF transformation may provide a theoretical direction for CAF-targeted therapy. Our experiments showed that DHA and ARM inhibited fibroblast-to-CAF transformation by suppressing PDGF-BB secretion from cancer cells, maintaining normal fibroblast function. Moreover, DHA and ARM inhibit tumor proliferation by maintaining normal fibroblast function and exert direct inhibitory effects on tumor cells (Figure 11). We further explored the effects of artemisinin derivatives on CAF deactivation and PDGF-BB signaling blockade, and the results indicated that artemisinin derivatives had no significant impact. These results suggest that artemisinin derivatives primarily regu-

late tumor cells rather than acting directly on CAFs. This phenomenon can be attributed to the more pronounced inhibitory effect of artemisinin derivatives on tumor cells than on normal cells [29]. We also found that hOMF cells were less sensitive to artemisinin derivatives than Cal-27 cells were during drug concentration screening. The selective cytotoxicity of artemisinin derivatives toward tumor cells minimizes their impact on normal cells, offering a potential research direction to address the current challenges of drug side effects in tumor-targeted therapies.

The safety of artemisinin derivatives as front-line antimalarial drugs has been widely recognized [55]. Studies have indicated that the drug concentrations required for antitumor and antimalarial effects differ significantly [41]. To address this, we determined safe dosages of DHA (dihydroartemisinin) and ARM (artemether) in BALB/c nude mice. Using a BALB/c nude mouse model of OTSCC, we observed that artemisinin derivatives, at safe dosages, significantly inhibited the progression of OTSCC. To further investigate the tumor burden induced by CAFs, we used a co-transplanted tumor model combining OTSCC cells and CAFs in BALB/c nude mice. This model revealed that CAFs significantly enhanced tumor volume. Further analyses demonstrated that artemisinin derivatives inhibited the secretion of PDGF-BB by cancer cells, normalizing fibroblasts and suppressing tumor progression in vivo. In addition, artemisinin derivatives have been found to inhibit tumor progression by directly suppressing the proliferation of tumor cells. Unlike conventional therapies that target stromal cells,

artemisinin derivatives exert their effects by directly targeting tumor cells, thereby influencing tumor-stroma interactions. This approach differs from current drug development strategies aimed at stromal cells, which often focus on mechanisms involving CAF-specific markers, such as fibroblast activation protein (FAP), or signaling pathways involving cytokines, such as transforming growth factor beta (TGF- β) and epidermal growth factor (ERGF) [56-58]. However, the regulatory role of tumor cells within the microenvironment appears to be overlooked, which may contribute to the clinical bottleneck faced by targeted therapies [59].

Artemisinin derivatives exhibit high selectivity for specific proteins in their biological activity. Network pharmacology studies have found that artemisinin derivatives can tightly bind to AKT1, EGFR, and NFKB1, exerting cytotoxic effects [60]. Related research indicates that artemisinin derivatives target and inhibit heat shock protein 90 (Hsp90), suppressing AKT and ERK signaling and contributing to their anti-tumor activity [61]. In gastric cancer studies, DHA was found to downregulate fibroblast growth factor 2 (FGF2), thereby inhibiting angiogenesis [62]. Further research has shown that as suitable ferroptosis inducers, artemisinin derivatives can induce tumor ferroptosis through multiple targeted pathways. Specifically, artemisinin derivatives induce tumor ferroptosis by modulating the ERK signaling pathway and downregulating the STAT3 signaling pathway [63, 64]. They can also trigger ferroptosis in primary hepatocellular carcinoma cells by upregulating CHAC1 [65]. Moreover, artemisinin compounds regulate iron homeostasis, making cancer cells more sensitive to ferroptosis [22]. These findings highlight the immense potential of artemisinin derivatives in cancer therapy. Studies suggest that artemisinin derivatives can improve polycystic ovary syndrome (PCOS) by directly targeting Lon protease 1 (LONP1) [66]. Artemisinin has also been reported to induce ferroptosis by regulating Atf3 or overexpressing Rock1, thereby reversing ovarian fibrosis (HF), further underscoring its potential as an anti-fibrotic agent [67].

Artesunate is a semisynthetic, water-soluble compound derived from the traditional Chinese medicine artemisinin, widely used in clinical settings to treat malaria [68]. A study involving

1,391 French patients showed a mortality rate of 4.1% among malaria patients treated with Artesunate, with 2% of the cases reporting adverse events related to death [69]. Currently, research on the clinical application of artemisinin derivatives in cancer therapy is limited. Still, small sample studies suggest that artemether does not exhibit significant side effects in the treatment of metastatic breast cancer [70]. Another study found that oral artemisinin effectively alleviated symptoms in patients with advanced metastatic cervical cancer [71]. However, it is essential to note that this conclusion does not rule out the potential side effects of artemisinin derivatives in cancer treatment. In a large number of clinical samples for anti-malarial treatment, artemisinin showed eosinophilia during short-term treatment, but this side effect is reversible after discontinuation of the medication [72]. Encouragingly, some studies suggest that artemisinin derivatives can selectively kill tumor cells while offering some protective effects on normal cells [73]. Therefore, further exploration into the protective mechanisms of artemisinin derivatives on normal cells could provide valuable insights for reducing clinical side effects. Additionally, bioengineering materials may offer new possibilities for the clinical use of artemisinin derivatives.

In summary, this study found that artemisinin derivatives exert a dual anti-tumor effect by directly regulating or inhibiting tumor cell proliferation, providing a theoretical basis for developing targeted drugs based on artemisinin derivatives. Although this study offers valuable insights, it also has some limitations. The tumor microenvironment is a highly dynamic system that involves processes such as angiogenesis, immune cell infiltration, the formation of pre-metastatic niches, and extracellular matrix remodeling [74-77]. These components collectively shape the tumor's biological characteristics and clinical manifestations. While indirect co-culture systems can somewhat simulate the signaling between different cell populations through solution exchange, they cannot replicate the direct contact and interactions between tumor cells and other cells. They cannot encompass the heterogeneity of CAFs (cancer-associated fibroblasts) in vivo [78]. This limitation restricts the accurate reproduction of complex cell-to-cell interactions within the tumor microenvironment. Although this study partially

compensates for the shortcomings of indirect in vitro culture through in vivo models, tumors are complex three-dimensional structures composed of various cell types. Future research will employ more sophisticated 3D co-culture systems and tumor organoids to overcome these limitations, allowing for a more realistic simulation of the tumor microenvironment. Additionally, the sample size used in each animal model group in this study is relatively small, which may reduce the generalizability of the results. In the future, we will overcome the sample size limitation to obtain more robust evidence and further validate the efficacy of artemisinin derivatives in cancer.

Acknowledgements

We thank the Science and Technology Incubation Centre of Kunming Medical University and the Yunnan Provincial Key Laboratory of Dentistry for providing the experimental platform, the National Natural Science Foundation of China for financial support (82060496, 82460520), and Editage for revising the manuscript.

Disclosure of conflict of interest

None.

Address correspondence to: Dr. Yongwen He, Kunming Medical University, Yunnan Key Laboratory of Stomatology, 1168, Chunrong West Road, Yuhua Street, Chenggong District, Kunming 650106, Yunnan, China. Tel: +86-13668796269; E-mail: kmmczb@163.com; kyyzb@kmmu.edu.cn; ynkqyy@163.com

References

- [1] Mody MD, Rocco JW, Yom SS, Haddad RI and Saba NF. Head and neck cancer. *Lancet* 2021; 398: 2289-2299.
- [2] Sung H, Ferlay J, Siegel RL, Laversanne M, Soerjomataram I, Jemal A and Bray F. Global cancer statistics 2020: GLOBOCAN estimates of incidence and mortality worldwide for 36 cancers in 185 countries. *CA Cancer J Clin* 2021; 71: 209-249.
- [3] Chow LQM. Head and neck cancer. *N Engl J Med* 2020; 382: 60-72.
- [4] Fang H and Declerck YA. Targeting the tumor microenvironment: from understanding pathways to effective clinical trials. *Cancer Res* 2013; 73: 4965-4977.
- [5] Roma-Rodrigues C, Mendes R, Baptista PV and Fernandes AR. Targeting tumor microenvironment for cancer therapy. *Int J Mol Sci* 2019; 20: 840.
- [6] Zhang H, Deng T, Liu R, Ning T, Yang H, Liu D, Zhang Q, Lin D, Ge S, Bai M, Wang X, Zhang L, Li H, Yang Y, Ji Z, Wang H, Ying G and Ba Y. CAF secreted miR-522 suppresses ferroptosis and promotes acquired chemo-resistance in gastric cancer. *Mol Cancer* 2020; 19: 43.
- [7] Tommelein J, Verset L, Boterberg T, Demetter P, Bracke M and De Wever O. Cancer-associated fibroblasts connect metastasis-promoting communication in colorectal cancer. *Front Oncol* 2015; 5: 63.
- [8] Dong L, Sun Q, Song F, Song X, Lu C, Li Y and Song X. Identification and verification of eight cancer-associated fibroblasts related genes as a prognostic signature for head and neck squamous cell carcinoma. *Heliyon* 2023; 9: e14003.
- [9] Nurmik M, Ullmann P, Rodriguez F, Haan S and Letellier E. In search of definitions: cancer-associated fibroblasts and their markers. *Int J Cancer* 2020; 146: 895-905.
- [10] Foster DS, Januszyk M, Delitto D, Yost KE, Griffin M, Guo J, Guardino N, Delitto AE, Chinta M, Burcham AR, Nguyen AT, Bauer-Rowe KE, Titan AL, Salhotra A, Jones RE, da Silva O, Lindsay HG, Berry CE, Chen K, Henn D, Mascharak S, Talbott HE, Kim A, Nosrati F, Sivaraj D, Ransom RC, Matthews M, Khan A, Wagh D, Collier J, Gurtner GC, Wan DC, Wapnir IL, Chang HY, Norton JA and Longaker MT. Multiomic analysis reveals conservation of cancer-associated fibroblast phenotypes across species and tissue of origin. *Cancer Cell* 2022; 40: 1392-1406, e7.
- [11] Wu X, Lu W, Zhang W, Zhang D, Mei H, Zhang M, Cui Y and Zhuo Z. Integrated analysis of single-cell RNA-seq and bulk RNA-seq unravels the heterogeneity of cancer-associated fibroblasts in TNBC. *Aging (Albany NY)* 2023; 15: 12674-12697.
- [12] Shangguan L, Ti X, Krause U, Hai B, Zhao Y, Yang Z and Liu F. Inhibition of TGF- β /Smad signaling by BAMBI blocks differentiation of human mesenchymal stem cells to carcinoma-associated fibroblasts and abolishes their protumor effects. *Stem Cells* 2012; 30: 2810-2819.
- [13] Zhang T, Li X, He Y, Wang Y, Shen J, Wang S, You Q, Zhai J and Shen L. Cancer-associated fibroblasts-derived HAPLN1 promotes tumour invasion through extracellular matrix remodeling in gastric cancer. *Gastric Cancer* 2022; 25: 346-359.
- [14] Fredriksson L, Li H and Eriksson U. The PDGF family: four gene products form five dimeric

Antitumor effects of artemisinin derivatives

- isoforms. *Cytokine Growth Factor Rev* 2004; 15: 197-204.
- [15] Homsí J and Daud AI. Spectrum of activity and mechanism of action of VEGF/PDGF inhibitors. *Cancer Control* 2007; 14: 285-294.
- [16] Xiu-Ying H, Yue-Xiang Z, Hui-Si Y, Hong-Zhou Y, Qing-Jie X and Ting-Hua W. PDGFBB facilitates tumorigenesis and malignancy of lung adenocarcinoma associated with PI3K-AKT/MAPK signaling. *Sci Rep* 2024; 14: 4191.
- [17] Hu H, Liu B, Zuo Y, Liu D, Xie R and Cui W. dl-3-n-butylphthalide suppresses PDGF-BB-stimulated vascular smooth muscle cells proliferation via induction of autophagy. *Life Sci* 2016; 151: 182-188.
- [18] Lee J, Termglinchan V, Diecke S, Itzhaki I, Lam CK, Garg P, Lau E, Greenhaw M, Seeger T, Wu H, Zhang JZ, Chen X, Gil IP, Ameen M, Sallam K, Rhee JW, Churko JM, Chaudhary R, Chour T, Wang PJ, Snyder MP, Chang HY, Karakikes I and Wu JC. Activation of PDGF pathway links LMNA mutation to dilated cardiomyopathy. *Nature* 2019; 572: 335-340.
- [19] Heldin CH, Lennartsson J and Westermark B. Involvement of platelet-derived growth factor ligands and receptors in tumorigenesis. *J Intern Med* 2018; 283: 16-44.
- [20] Kobayashi H, Enomoto A, Woods SL, Burt AD, Takahashi M and Worthley DL. Cancer-associated fibroblasts in gastrointestinal cancer. *Nat Rev Gastroenterol Hepatol* 2019; 16: 282-295.
- [21] Tu Y. Artemisinin-a gift from traditional Chinese medicine to the world (nobel lecture). *Angew Chem Int Ed Engl* 2016; 55: 10210-10226.
- [22] Chen GQ, Benthani FA, Wu J, Liang D, Bian ZX and Jiang X. Artemisinin compounds sensitize cancer cells to ferroptosis by regulating iron homeostasis. *Cell Death Differ* 2020; 27: 242-254.
- [23] Slezakova S and Ruda-Kucerova J. Anticancer activity of artemisinin and its derivatives. *Anticancer Res* 2017; 37: 5995-6003.
- [24] Roy S, He R, Kapoor A, Forman M, Mazzone JR, Posner GH and Arav-Boger R. Inhibition of human cytomegalovirus replication by artemisinins: effects mediated through cell cycle modulation. *Antimicrob Agents Chemother* 2015; 59: 3870-3879.
- [25] Zhou X, Soto-Gamez A, Nijdam F, Setroikromo R and Quax WJ. Dihydroartemisinin-transferrin adducts enhance TRAIL-induced apoptosis in triple-negative breast cancer in a P53-independent and ROS-dependent manner. *Front Oncol* 2022; 11: 789336.
- [26] Pirali M, Taheri M, Zarei S, Majidi M and Ghafouri H. Artesunate, as a HSP70 ATPase activity inhibitor, induces apoptosis in breast cancer cells. *Int J Biol Macromol* 2020; 164: 3369-3375.
- [27] Cabello CM, Lamore SD, Bair WB 3rd, Qiao S, Azimian S, Lesson JL and Wondrak GT. The redox antimalarial dihydroartemisinin targets human metastatic melanoma cells but not primary melanocytes with induction of NOXA-dependent apoptosis. *Invest New Drugs* 2012; 30: 1289-1301.
- [28] Yuan B, Liao F, Shi ZZ, Ren Y, Deng XL, Yang TT, Li DY, Li RF, Pu DD, Wang YJ, Tan Y, Yang Z and Zhang YH. Dihydroartemisinin inhibits the proliferation, colony formation and induces ferroptosis of lung cancer cells by inhibiting PRIM2/SLC7A11 axis. *Onco Targets Ther* 2020; 13: 10829-10840.
- [29] Roh JL, Kim EH, Jang H and Shin D. Nrf2 inhibition reverses the resistance of cisplatin-resistant head and neck cancer cells to artesunate-induced ferroptosis. *Redox Biol* 2017; 11: 254-262.
- [30] Xiao X, Li Y, Wang Y, Zhang Y, Chen J, Liu W, Tang J, Yue F and Yang J. Dihydroartemisinin inhibits lewis lung carcinoma progression by inducing macrophages M1 polarization via AKT/mTOR pathway. *Int Immunopharmacol* 2022; 103: 108427.
- [31] Yu R, Jin L, Li F, Fujimoto M, Wei Q, Lin Z, Ren X, Jin Q, Li H, Meng F and Jin G. Dihydroartemisinin inhibits melanoma by regulating CTL/treg anti-tumor immunity and STAT3-mediated apoptosis via IL-10 dependent manner. *J Dermatol Sci* 2020; 99: 193-202.
- [32] Wang CZ, Wan C, Luo Y, Zhang CF, Zhang QH, Chen L, Liu Z, Wang DH, Lager M, Li CH, Jiang TL, Hou L and Yuan CS. Effects of dihydroartemisinin, a metabolite of artemisinin, on colon cancer chemoprevention and adaptive immune regulation. *Mol Biol Rep* 2022; 49: 2695-2709.
- [33] Mancuso RI, Olalla Saad ST and Azambuja JH. Artesunate switches monocytes to an inflammatory phenotype with the ability to kill leukemic cells. *Int J Mol Sci* 2021; 22: 608.
- [34] Kanlaya R, Peerapen P, Nilnumkhum A, Plumworasawat S, Sueksakit K and Thongboonkerd V. Epigallocatechin-3-gallate prevents TGF- β 1-induced epithelial-mesenchymal transition and fibrotic changes of renal cells via GSK-3 β / β -catenin/Snail1 and Nrf2 pathways. *J Nutr Biochem* 2020; 76: 108266.
- [35] Kanlaya R, Subkod C, Nanthawuttiphan S and Thongboonkerd V. Caffeine prevents oxalate-induced epithelial-mesenchymal transition of renal tubular cells by its anti-oxidative property through activation of Nrf2 signaling and suppression of Snail1 transcription factor. *Biomed Pharmacother* 2021; 141: 111870.

Antitumor effects of artemisinin derivatives

- [36] Nemzek JA, Hakenjos JM, Hoenerhoff MJ and Fry CD. Isoflurane and pentobarbital anesthesia for pulmonary studies requiring prolonged mechanical ventilation in mice. *J Am Assoc Lab Anim Sci* 2024; 63: 41-48.
- [37] Li H, Liu C, Li R, Zhou L, Ran Y, Yang Q, Huang H, Lu H, Song H, Yang B, Ru H, Lin S and Zhang L. AARS1 and AARS2 sense L-lactate to regulate cGAS as global lysine lactyltransferases. *Nature* 2024; 634: 1229-1237.
- [38] Pérttega-Gomes N, Vizcaíno JR, Attig J, Jurmeister S, Lopes C and Baltazar F. A lactate shuttle system between tumour and stromal cells is associated with poor prognosis in prostate cancer. *BMC Cancer* 2014; 14: 352.
- [39] Tobar N, Porras O, Smith PC, Barros LF and Martínez J. Modulation of mammary stromal cell lactate dynamics by ambient glucose and epithelial factors. *J Cell Physiol* 2017; 232: 136-144.
- [40] Zheng S, Wu R, Deng Y and Zhang Q. Dihydroartemisinin represses oral squamous cell carcinoma progression through downregulating mitochondrial calcium uniporter. *Bioengineered* 2022; 13: 227-241.
- [41] Sun C, Cao Y, Zhu P and Zhou B. A mitochondria-targeting artemisinin derivative with sharply increased antitumor but depressed anti-yeast and anti-malaria activities. *Sci Rep* 2017; 7: 45665.
- [42] Hosaka K, Yang Y, Seki T, Fischer C, Dubey O, Fredlund E, Hartman J, Religa P, Morikawa H, Ishii Y, Sasahara M, Larsson O, Cossu G, Cao R, Lim S and Cao Y. Pericyte-fibroblast transition promotes tumor growth and metastasis. *Proc Natl Acad Sci U S A* 2016; 113: E5618-5627.
- [43] Chronopoulos A, Robinson B, Sarper M, Cortes E, Auernheimer V, Lachowski D, Attwood S, García R, Ghassemi S, Fabry B and Del Río Hernández A. ATRA mechanically reprograms pancreatic stellate cells to suppress matrix remodelling and inhibit cancer cell invasion. *Nat Commun* 2016; 7: 12630.
- [44] Zervantonakis IK, Poskus MD, Scott AL, Selfors LM, Lin JR, Dillon DA, Pathania S, Sorger PK, Mills GB and Brugge JS. Fibroblast-tumor cell signaling limits HER2 kinase therapy response via activation of MTOR and antiapoptotic pathways. *Proc Natl Acad Sci U S A* 2020; 117: 16500-16508.
- [45] Mizutani Y, Kobayashi H, Iida T, Asai N, Masamune A, Hara A, Esaki N, Ushida K, Mii S, Shiraki Y, Ando K, Weng L, Ishihara S, Ponik SM, Conklin MW, Haga H, Nagasaka A, Miyata T, Matsuyama M, Kobayashi T, Fujii T, Yamada S, Yamaguchi J, Wang T, Woods SL, Worthley D, Shimamura T, Fujishiro M, Hirooka Y, Enomoto A and Takahashi M. Meflin-positive cancer-associated fibroblasts inhibit pancreatic carcinogenesis. *Cancer Res* 2019; 79: 5367-5381.
- [46] Shen T, Li Y, Zhu S, Yu J, Zhang B, Chen X, Zhang Z, Ma Y, Niu Y and Shang Z. YAP1 plays a key role of the conversion of normal fibroblasts into cancer-associated fibroblasts that contribute to prostate cancer progression. *J Exp Clin Cancer Res* 2020; 39: 36.
- [47] Meng W, Wu Y, He X, Liu C, Gao Q, Ge L, Wu L, Liu Y, Guo Y, Li X, Liu Y, Chen S, Kong X, Liang Z and Zhou H. A systems biology approach identifies effective tumor-stroma common targets for oral squamous cell carcinoma. *Cancer Res* 2014; 74: 2306-2315.
- [48] Alkasalias T, Flaberg E, Kashuba V, Alexeyenko A, Pavlova T, Savchenko A, Szekely L, Klein G and Guven H. Inhibition of tumor cell proliferation and motility by fibroblasts is both contact and soluble factor dependent. *Proc Natl Acad Sci U S A* 2014; 111: 17188-17193.
- [49] Hauge A and Rofstad EK. Antifibrotic therapy to normalize the tumor microenvironment. *J Transl Med* 2020; 18: 207.
- [50] Yin Z, Dong C, Jiang K, Xu Z, Li R, Guo K, Shao S and Wang L. Heterogeneity of cancer-associated fibroblasts and roles in the progression, prognosis, and therapy of hepatocellular carcinoma. *J Hematol Oncol* 2019; 12: 101.
- [51] Lappano R, Rigidacciolo DC, Belfiore A, Maggioni M and De Francesco EM. Cancer associated fibroblasts: role in breast cancer and potential as therapeutic targets. *Expert Opin Ther Targets* 2020; 24: 559-572.
- [52] Miao L, Guo S, Lin CM, Liu Q and Huang L. Nanoformulations for combination or cascade anticancer therapy. *Adv Drug Deliv Rev* 2017; 115: 3-22.
- [53] Chen Q, Chen L, Kong D, Shao J, Wu L and Zheng S. Dihydroartemisinin alleviates bile duct ligation-induced liver fibrosis and hepatic stellate cell activation by interfering with the PDGF- β R/ERK signaling pathway. *Int Immunopharmacol* 2016; 34: 250-258.
- [54] Henderson NC, Rieder F and Wynn TA. Fibrosis: from mechanisms to medicines. *Nature* 2020; 587: 555-566.
- [55] Li Y, Shan NN and Sui XH. Research progress on artemisinin and its derivatives against hematological malignancies. *Chin J Integr Med* 2020; 26: 947-955.
- [56] Zhou S, Zhen Z, Paschall AV, Xue L, Yang X, Bebin-Blackwell AG, Cao Z, Zhang W, Wang M, Teng Y, Zhou G, Li Z, Avci FY, Tang W and Xie J. FAP-targeted photodynamic therapy mediated by ferritin nanoparticles elicits an immune response against cancer cells and cancer associated fibroblasts. *Adv Funct Mater* 2021; 31: 2007017.

Antitumor effects of artemisinin derivatives

- [57] Mazzocca A, Fransvea E, Dituri F, Lupo L, Antonaci S and Giannelli G. Down-regulation of connective tissue growth factor by inhibition of transforming growth factor beta blocks the tumor-stroma cross-talk and tumor progression in hepatocellular carcinoma. *Hepatology* 2010; 51: 523-534.
- [58] Álvarez-Teijeiro S, García-Inclán C, Villaronga MÁ, Casado P, Hermida-Prado F, Granda-Díaz R, Rodrigo JP, Calvo F, Del-Río-Ibáñez N, Gandarillas A, Morís F, Hermsen M, Cutillas P and García-Pedrero JM. Factors secreted by cancer-associated fibroblasts that sustain cancer stem properties in head and neck squamous carcinoma cells as potential therapeutic targets. *Cancers (Basel)* 2018; 10: 334.
- [59] Nahas G, Bliss SA, Sinha G, Ganta T, Greco SJ and Rameshwar P. Is reduction of tumor burden sufficient for the 21st century? *Cancer Lett* 2015; 356: 149-155.
- [60] Hung Truong N, Hung Nguyen P, Nghi Do H, Ha Nguyen X, Loc Vu T, Hai Pham T, Trang Luu H, Cuong Nguyen M and Luu VC. Synthesis and cytotoxic activities of novel ether conjugates of dihydroartemisinin and zerumbone: evidenced by integrating network pharmacology and in vitro assay. *Chem Biodivers* 2025; 22: e202401571.
- [61] Yuan-Ce L, Qi Z, Hong-Yang Z, Yan-Wen W, Yu-Mei S, Bi-Juan Y and Jun-Lin Y. Artesunate, as an Hsp90 inhibitor, inhibits the proliferation of burkitt's lymphoma cells by inhibiting AKT and ERK. *Front Pharmacol* 2023; 14: 1218467.
- [62] Wang H, Ding Q, Zhou H, Huang C, Liu G, Zhao X, Cheng Z and You X. Dihydroartemisinin inhibited vasculogenic mimicry in gastric cancer through the FGF2/FGFR1 signaling pathway. *Phytomedicine* 2024; 134: 155962.
- [63] Song Q, Peng S, Che F and Zhu X. Artesunate induces ferroptosis via modulation of p38 and ERK signaling pathway in glioblastoma cells. *J Pharmacol Sci* 2022; 148: 300-306.
- [64] Guo W, Liu Y, Chen B and Fan L. Target prediction and potential application of dihydroartemisinin on hepatocarcinoma treatment. *Naunyn Schmiedeberg's Arch Pharmacol* 2024; 397: 7711-7724.
- [65] Wang Z, Li M, Liu Y, Qiao Z, Bai T, Yang L and Liu B. Dihydroartemisinin triggers ferroptosis in primary liver cancer cells by promoting and unfolded protein response-induced upregulation of CHAC1 expression. *Oncol Rep* 2021; 46: 240.
- [66] Liu Y, Jiang JJ, Du SY, Mu LS, Fan JJ, Hu JC, Ye Y, Ding M, Zhou WY, Yu QH, Xia YF, Xu HY, Shi YJ, Qian SW, Tang Y, Li W, Dang YJ, Dong X, Li XY, Xu CJ and Tang QQ. Artemisinins ameliorate polycystic ovarian syndrome by mediating LONP1-CYP11A1 interaction. *Science* 2024; 384: eadk5382.
- [67] Wang Y, Li Y, Qiu Y, Shen M, Wang L, Shao J, Zhang F, Xu X, Zhang Z, Guo M and Zheng S. Artesunate induces ferroptosis in hepatic stellate cells and alleviates liver fibrosis via the ROCK1/ATF3 axis. *J Clin Transl Hepatol* 2024; 12: 36-51.
- [68] Zhang M, Lin J, Zhang J, Zhao R, Wan J and Nong Y. Artesunate inhibits airway remodeling in asthma via the MAPK signaling pathway. *Front Pharmacol* 2023; 14: 1145188.
- [69] Roussel C, Ndour PA, Kendjo E, Larréché S, Taieb A, Henry B, Lebrun-Vignes B, Chambrión C, Argy N, Houzé S, Mouri O, Courtin D, Angoulvant A, Delacour H, Gay F, Siriez JY, Danis M, Bruneel F, Bouchaud O, Caumes E, Piarroux R, Thellier M, Jauréguiberry S and Buffet P; FRENCH Artesunate Working Group. Intravenous artesunate for the treatment of severe imported malaria: implementation, efficacy, and safety in 1391 patients. *Clin Infect Dis* 2021; 73: 1795-1804.
- [70] König M, von Hagens C, Hoth S, Baumann I, Walter-Sack I, Edler L and Sertel S. Investigation of ototoxicity of artesunate as add-on therapy in patients with metastatic or locally advanced breast cancer: new audiological results from a prospective, open, uncontrolled, monocentric phase I study. *Cancer Chemother Pharmacol* 2016; 77: 413-427.
- [71] Ferrall L, Lin KY, Roden RBS, Hung CF and Wu TC. Cervical cancer immunotherapy: facts and hopes. *Clin Cancer Res* 2021; 27: 4953-4973.
- [72] Tshetu AK, Gaye O, Kayentao K, Thompson R, Bhatt KM, Sesay SS, Bustos DG, Tjitra E, Bedu-Addo G, Borghini-Fuhrer I, Duparc S, Shin CS and Fleckenstein L; Pyronaridine-artesunate Study Team. Efficacy and safety of a fixed-dose oral combination of pyronaridine-artesunate compared with artemether-lumefantrine in children and adults with uncomplicated *Plasmodium falciparum* malaria: a randomised non-inferiority trial. *Lancet* 2010; 375: 1457-1467.
- [73] Kiani BH, Kayani WK, Khayam AU, Dilshad E, Ismail H and Mirza B. Artemisinin and its derivatives: a promising cancer therapy. *Mol Biol Rep* 2020; 47: 6321-6336.
- [74] Zhang Q, Wang C, Li R, Liu J, Wang J, Wang T and Wang B. The BAP31/miR-181a-5p/RECK axis promotes angiogenesis in colorectal cancer via fibroblast activation. *Front Oncol* 2023; 13: 1056903.
- [75] Lakins MA, Ghorani E, Munir H, Martins CP and Shields JD. Cancer-associated fibroblasts induce antigen-specific deletion of CD8 + T cells to protect tumour cells. *Nat Commun* 2018; 9: 948.

Antitumor effects of artemisinin derivatives

- [76] Kong J, Tian H, Zhang F, Zhang Z, Li J, Liu X, Li X, Liu J, Li X, Jin D, Yang X, Sun B, Guo T, Luo Y, Lu Y, Lin B and Liu T. Extracellular vesicles of carcinoma-associated fibroblasts creates a pre-metastatic niche in the lung through activating fibroblasts. *Mol Cancer* 2019; 18: 175.
- [77] Akinjiyan FA, Ibitoye Z, Zhao P, Shriver LP, Patti GJ, Longmore GD and Fuh KC. DDR2-regulated arginase activity in ovarian cancer-associated fibroblasts promotes collagen production and tumor progression. *Oncogene* 2024; 43: 189-201.
- [78] Waise S, Parker R, Rose-Zerilli MJJ, Layfield DM, Wood O, West J, Ottensmeier CH, Thomas GJ and Hanley CJ. An optimised tissue disaggregation and data processing pipeline for characterising fibroblast phenotypes using single-cell RNA sequencing. *Sci Rep* 2019; 9: 9580.